Tectonic evolution of the abrupt northern termination of the Sistan Suture Zone (eastern Iran)

Emad Rojhani[a, e], Farzin Ghaemi*[a], Sasan Bagheri[b], Shihu Li[c], Nalan Lom[d],[e] , Douwe J.J. van Hinsbergen[e]

[a]Department of Geology, Faculty of Science, Ferdowsi University of Mashhad, Mashhad, Iran,

[b]Department of Geoscience, Faculty of Science, University of Sistan and Baluchestan, Zahedan, Iran,

[c]State Key Laboratory of Lithospheric and Environmental Coevolution, Institute of Geology and Geophysics, Chinese Academy of Sciences, Beijing, 100029, China,

[d]Institute of Earth Sciences, Heidelberg University, Heidelberg, 69117, Germany

[e]Department of Earth Sciences, Utrecht University, Utrecht, the Netherlands,

Emad Rojhani: Writing - Original Draft, Formal analysis, Methodology, Investigation **Farzin Ghaemi**: Supervision, Funding acquisition **Sasan Bagheri**: Conceptualization, Methodology, Project administration **Shihu Li**: Resources, Investigation, Writing - Review & Editing, **Nalan Lom**: Writing - Review & Editing, **Douwe J.J. van Hinsbergen**: Conceptualization, Writing - Original Draft, Writing - Review & Editing, Investigation.

Corresponding author: Farzin Ghaemi (fghaeemi@um.ac.ir)

Highlights:

- The ocean-derived accretionary prism of the Sistan suture zone terminates abruptly in the north against suture-perpendicular Madar-Kuh fault system
- The Madar-Kuh fault is currently a steep thrust that emplaced the Lut block margin over the suture zone rocks
- This thrust is Eocene in age, and its curvilinear appearance is the result of younger, small-scale refolding
- During Cretaceous-Eocene Sistan subduction, the Madar-Kuh fault was a STEP fault, accommodating Helmand Block extrusion from western Tibet.

Abstract

The Sistan Suture Zone in eastern Iran hosts the remains of an ocean basin that subducted between the Iranian Lut Block and the Helmand Block in Late Cretaceous to early Eocene time. Surprisingly, this suture zone is N-S trending, nearly perpendicular to and north of the overall E-W trending Neo-Tethyan suture zone that represents the main regional subduction system. Here, we show that the main N-S trend of the suture, defined by folds and thrusts of a westward and structurally downward-younging ocean-derived accretionary prism, abruptly ends against the steep Madar-Kuh thrust. This thrust strikes nearly perpendicular to the Sistan accretionary prism. It disappears where also the accretionary prism disappears to the southwest, but continues beyond the suture zone towards the northeast showing a genetic relation to the former Sistan subduction zone. The Madar-Kuh thrust emplaces continental rocks of the Lut block over the oceanic domain. We show that thrust-parallel folds and thrusts were refolded, giving the Madar-Kuh Fault a curvilinear trend. Radial mafic dikes that are systematically strike-perpendicular to the first-generation folds returned U/Pb ages of 51.3±1.5 Ma and 43.1±0.5 Ma, showing that refolding occurred after the Sistan Suture closure. During Sistan ocean subduction, the Madar-Kuh Fault was a trench-perpendicular, subduction-parallel, straight fault at which subduction terminated: we interpret this as a subduction transform edge propagator (STEP) fault that accommodated westward motion of the Helmand Block into the Iranian back-arc region. Our findings provide key clues on microplates and continents that converged and collided within the Iranian upper plate of the Neo-Tethys subduction zone, and highlights that major and long-lived E-W component of tectonic motion along the southern Eurasian margin involved crustal extrusion away from western Tibet and into the Iranian back-arc basins, impacting the tectonic evolution of the Iranian and Tibetan plateaus alike.

Keywords: Sistan Suture Zone, subduction transform edge propagator (STEP), Tibetan extrusion, Neo-Tethys, Helmand Block

1. Introduction

Several major orogenic belts that formed during closure of the Neo-Tethys ocean experienced lateral extrusion of upper plate, orogenic lithosphere. Well-known examples are Anatolia migrating westward away from the Arabia-Eurasia collision zone (e.g., Jackson & McKenzie, 1984), the eastern Alps and northern Pannonian basin escaping from the Adria-Eurasia collision zone (e.g., Ratschbacher et al., 1991), and Indochina escaping eastwards from the India-Asia collision zone (e.g., Tapponnier et al., 1982; Li et al., 2017). Such lateral escape generates a non-cylindrical distribution of orogenic shortening and is accommodated along major strike-slip systems that may pose major seismic hazard.

A possible fourth major region of past lateral escape may have occurred in the central Neo-Tethyan region, affecting the tectonics of much of Afghanistan and eastern Iran. Tapponnier et al. (1981) already noticed that the first-order structural architecture of strike-slip faults surrounding the Helmand Block that occupies much of Afghanistan bears characteristics of westward escape, but scarcity of geological data from this region has prohibited the development of quantitative restorations of westward motion of the Helmand block.

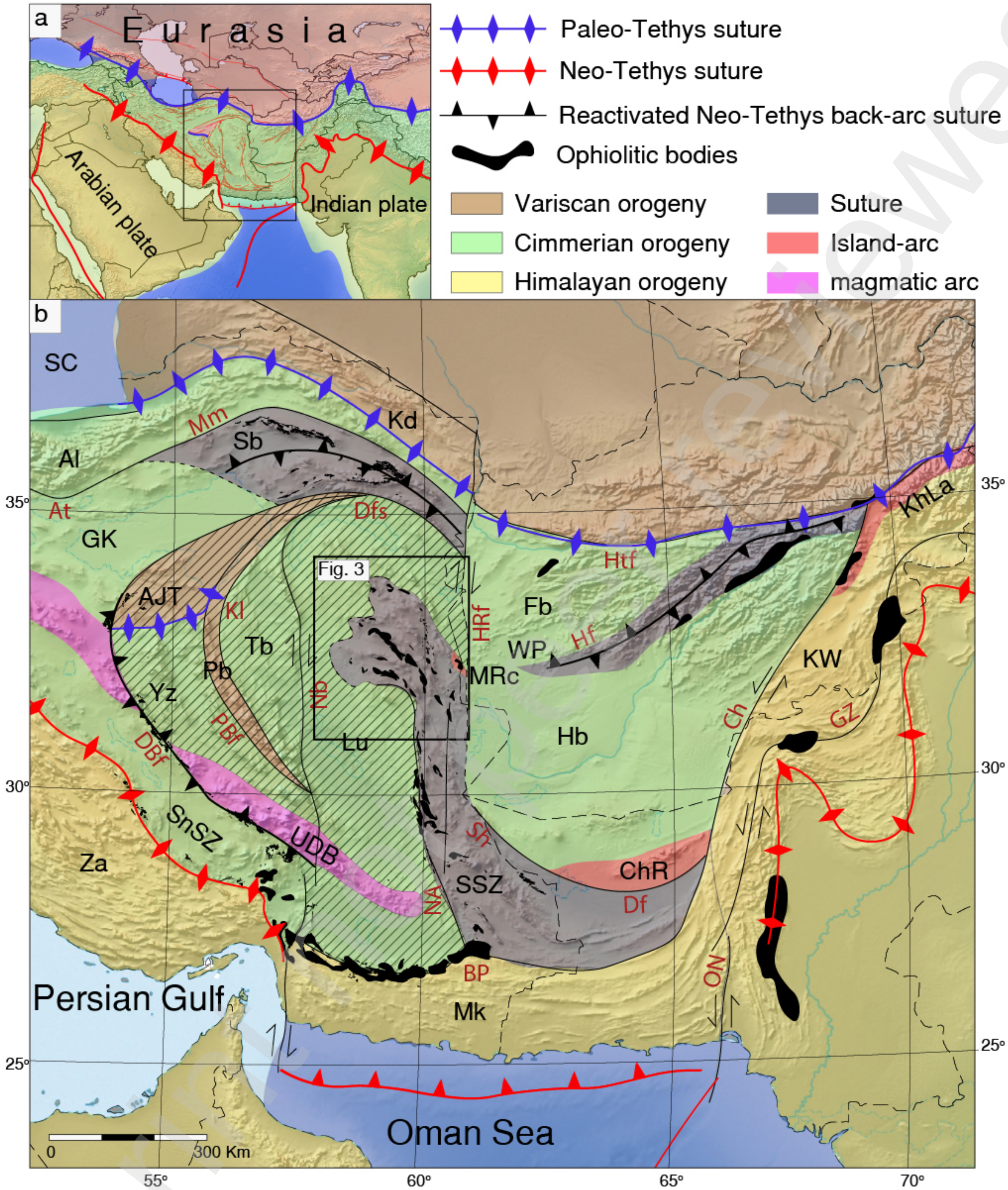

Figure 1. a) Location of the Sistan Suture Zone (SSZ) within the central Neo-Tethyan orogenic belt; b) The Sistan Suture Zone and surrounding tectonic blocks and sutures within the upper plate of the (former) Neo-Tethyan subduction system. Abbreviations: Al: Alborz, CEIM = Central-Eastern Iranian Microcontinnet; Fb: Farah Basin, GK: Great Kavir basin, HRf: HariRud Fault system; KD: Kopeht Dagh, Nh: Neh Fault, MRc: Mahi-Rud complex, Sb: Sabzevar, SC: South Caspian sea, SnSZ: Sanandaj-Sirjan Zone, SSZ: Sistan Suture Zone, UDMA: Urumieh-Dokhtar magmatic arc; WPS: Waras-Panjaw Suture.

The geology of eastern Iran may shed light on the role of lateral escape of the Helmand Block. There, the Sistan Suture is a prominent yet enigmatic, N-S trending 800 km long suture zone that separates the Helmand Block in the east from the Lut Block in the west (Figure 1). The N-S orientation of this suture zone is surprising because the closure of the Neo-Tethys Ocean that governed most of the orogenic architecture of the Alpine-Himalayan mountain belt has been dominated by N-S convergence and E-W trending subduction zones (e.g., Stampfli et al., 1991). Structural geological observations and distributions of metamorphic and arc magmatic rocks have led previous researchers to conclude that the subduction that closed the Sistan Suture Zone accommodated E-W convergence instead, between the Late Cretaceous and the Eocene (Agard et al., 2009; Angiboust et al., 2013; Arjmandzadeh et al., 2011; Bröcker et al., 2013; 2022; Saccani et al., 2010; Tirrul et al., 1983; Bagheri and Damani Gol, 2020; Jentzer, et al., 2022). Such E-W convergence closing the Sistan suture would require that the Helmand block was originally located much farther east than today, i.e. within the Karakoram-Tibetan realm, and moved westwards, in the upper plate of, and roughly parallel to the overall trend of the Neo-Tethyan subduction zone (Bagheri and Damani Gol, 2020). Such motions have mostly been conceptually inferred without detailed reconstruction, and in absence of further kinematic constraints the magnitude of the presumed Helmand extrusion is difficult to constrain. For instance, Bagheri and Damani Gol (2020) recently hypothesized that the Sistan Suture Zone was originally the ~E-W striking Neo-Tethyan trench that became oroclinally buckled over 180° (Figure 2a).

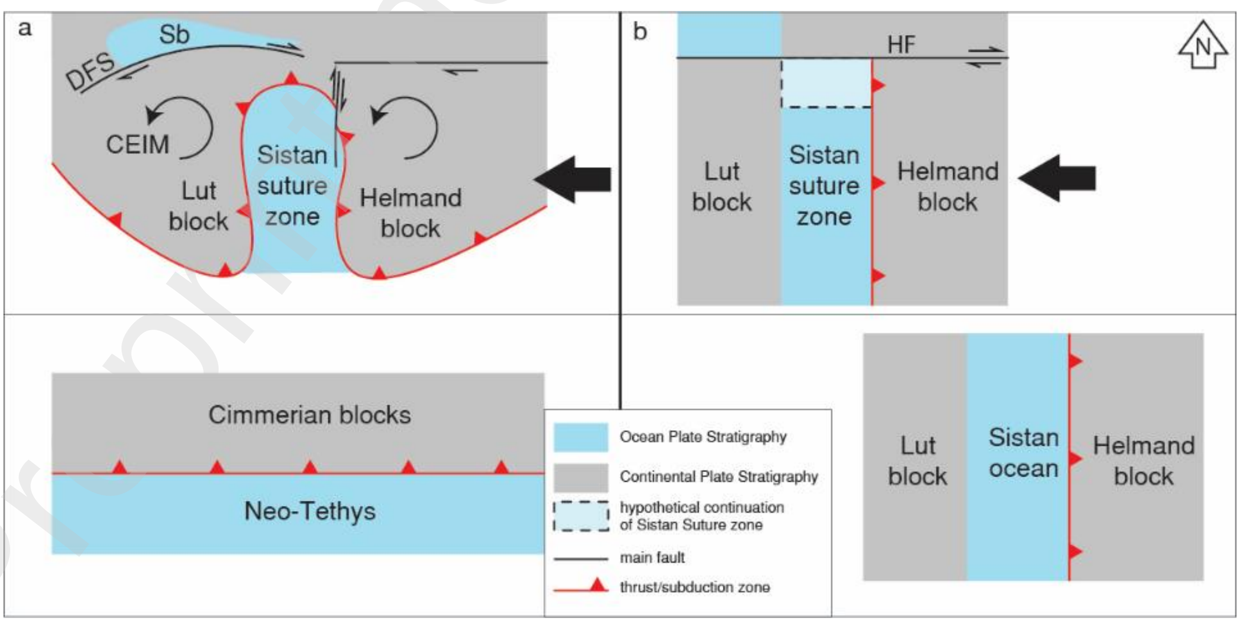

Figure 2. Simplified cartoon of two alternative explanations for northern termination of Sistan Suture Zone, a) the oroclinal buckling, b) the westward migration by transform faults. CEIM: Central-East Iranian Microcontinent, Sb: Sabzevar basin; main faults: DFS: Doruneh Fault System, WPS: Waras-Panjaw Suture.

Such a hypothesis would predict that the Sistan Suture Zone is symmetric belt connected with a tight orocline in the north. Alternatively, if the Sistan Suture Zone is not the result of oroclinal buckling but was always N-S striking, it either extended farther north than generally mapped (Rossetti et al., 2010), or should have ended against a transform plate boundary in the north (Figure 2b). In other words, the geological architecture of the northern termination of the Sistan Suture Zone holds the key to reconstruct the way in which E-W convergence between the Helmand and Lut Blocks was accommodated, and towards kinematically reconstructing these motions to infer the underlying dynamic drivers.

In this paper, we report the results of a field-based study into the structure and evolution of the northern termination of the Sistan Suture Zone, aiming to establish the location of the former subduction zone, the presence or absence of curvilinear belts and strike-slip faults surrounding this termination, and on the stratigraphic and magmatic architecture of this region to constrain the timing of deformation. We will develop our results into the implications for the tectonic evolution of the microplates within the upper plate of the Neo-Tethyan subduction system, and the role of tectonic extrusion in their history.

2. Geological setting

The geology of Iran and Afghanistan consists of blocks of continental crust that once formed a microcontinent kown as the ‘Cimmerian Continent’ that broke off Gondwana in the Permian opening the Neo-Tethys Ocean, and colliding with Eurasia in the Triassic closing the Paleotethys Ocean (Krumsiek, 1976; Şengör, 1979, 1984; Stampfli et al., 1991). Subsequently, the Neo-Tethys started subducting along the southern margin of the Cimmerian continent in Jurassic time until arrival of Arabian continental crust in the Paleogene (Berberian & King, 1981, Agard et al., 2011; McQuarrie and van Hinsbergen, 2013). In the upper plate of this subduction system, the Cimmerian continent became extended, and back-arc ocean basins formed in Jurassic to early Cretaceous time that subsequently closed in the Eocene and the Sistan suture is thought to be one of such ocean basins (Angiboust et al., 2013; Jentzer et al., 2022; Tirrul et al., 1983).

The Cimmerian continental blocks have a Precambrian crystaline basement that correlates well with the basement of Arabia (Berberian, 1973; Stöcklin, 1968, 1974; Stöcklin & Mabavi, 1973; Gass, 1977). The Paleotethys suture zone, with Paleozoic oceanic rocks is located in northern Iran and Afghanistan (Şengör, 1979). The Neo-Tethys suture zone is located in southern Iran, north of the Arabian margin-derived Zagros fold-thrust belt (Şengör, 1979; Berberian & King, 1981) (Figure 1) and south of a Jurassic to Eocene arc that intruded the Cimmerian (the Sanandaj-Sirjan and Urumieh Dokhtar arcs) (Agard et al., 2011; Berberian & Berberian, 1981; Stöcklin, 1968; Hassanzadeh & Wernicke, 2016).

The Cimmerian continent is now separated into several fault-bounded fragments and intervening, discontinuous suture zones. The Sanandaj-Sirjan arc and Alborz mountains are part of a western fragment that is bounded from the Central-East Iranian Microcontinent (CEIM), which consists of several crustal blocks separated by Cenozoic strike-slip faults (Walker & Jackson, 2004). The eastern of these fault bounded units is the Lut Block (Soffel & Förster, 1984) which is often used to denominator for the entire CEIM. The Lut Block exposes upper Proterozoic-Cambrian basement overlain by Paleozoic-Cenozoic sedimentary rocks and volcanics (Stöcklin, 1968; 1974; 1981). Triassic-Jurassic marine rocks are partly metamorphosed and locally intruded by Middle Jurassic to Cenozoic intrusions, and overlain by associated volcanic rocks (Esmaeily et al., 2005; Moradi Noghondar et al., 2011; Tarkian et al., 1983; Karimpour et al., 2011). These volcanics are interlayered with a thick shallow marine sequence, just west of the Sistan Suture Zone in particular by a thick Upper Cretaceous (upper Aptian-Cenomanian) Paleocene shelf limestone sequence that are also found to the northeast of the termination of the Sistan suture (Figure 3) (Alavi-Naini, 1980; Alavi-Naini & Behruzi, 1983; Eftekhar-Nezhad & Ruttner, 1977; Kluyver et al., 1983; Latifi et al., 2018; Raisossadat et al., 2020). These are overlain by Paleocene carbonates, unconformably overlying middle Eocene-Oligocene continental red beds and deformed Oligocene-Pliocene volcano-sedimentary rocks (Akrami et al., 2005).

Paleomagnetic data have reveals that the CEIM rocks suggest that the CEIM underwent large-scale rotation since the Jurassic, perhaps up to 90° (Davoudzadeh et al., 1981; Bina et al., 1986; Conrad et al., 1981; Mattei et al.., 2012; 2015; Soffel & Förster, 1980; Soffel et al., 1992, 1996).

The CEIM is surrounded by discontinuous belts of accreted oceanic rocks and ophiolites (Figure 1). These include the Inner Zagros suture zone in the south and the Sabsevar suture in the north, both with Cretaceous oceanic rocks (e.g., Moghadam & Stern, 2015; Pirnia et al., 2020; Rossetti et al., 2014). These sutures are connected the Great Kavir-Dorouneh strike-slip fault system (Bagheri and Stampfli, 2008). The Lut Block is bounded in the east by the Sistan Suture Zone from the Helmand Block of Afghanistan (Stöcklin, 1968). The Sistan Suture Zone contains ophiolites and accreted oceanic rocks of Cretaceous age and is commonly interpreted to have been derived from Cretaceous back-arc basins that formed in the upper plate of the subducting Neo-Tethyan subduction zone (Baroz et al, 1984; Arvin and Robinson, 1994; Shojaat et al., 2003; Ghazi et al., 2004; Rossetti et al., 2010; Zarrinkoub et al., 2012), although others have hypothesized that these ophiolite belts represent the Neo-Tethyan suture (Bagheri & Damani Gol, 2020; Moghadam & Stern, 2015).

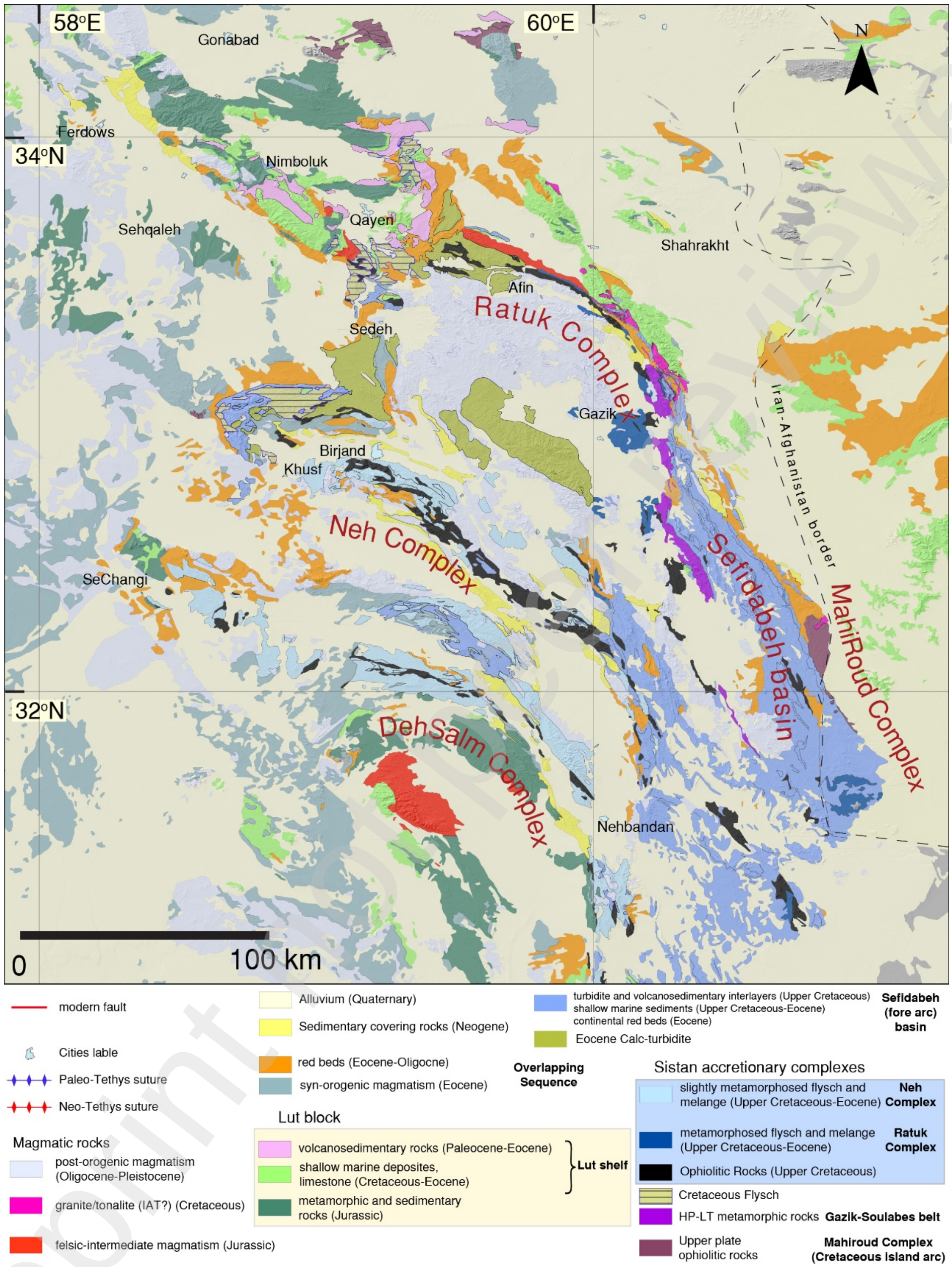

Figure 3. Geological map of northern termination of the Sistan Suture Zone, surrounded by the Lut Block in the northwest and west, and the Helmand block in the east (after Eftekhar-Nezhad and Ruttner, 1977; Alavi-Naini, 1980; Alavi-Naini and Behruzi, 1983; Guillou et al., 1983; Berthiaux et al., 1991; Eftekhar-Nezhad and Stöcklin, 1992).

The Helmand Block also consists of a Precambrian crystalline basement and is overlain by a Permian-middle Cenozoic, discontinuous, shallow-water carbonate sequence (Schreiber et al., 1972; Stöcklin, 1989). The basement of the Helmand Block is, as far as known, similar to the Cimmerian basement of Iran, but could as well correlate to the basement of the Qiangtang or Lhasa terranes of Tibet that are also derived from the northern Gondwana margin (Yin and Harrison, 2000; Kapp and DeCelles, 2019). Thie Helmand block is separated from Eurasia by the ophiolite-bearing Waras-Panjaw suture zone, and a wide, Triassic to lower Cretaceous flysch belt known as the Farah, or Farah Rud Basin, which overlies continental crust belongs to the Cimmerian block (in Afghanistan known as the Band-e Bayan block (Boulin, 1990; Montenat, 2009; Siehl, 2017). The Band-e Bayan block is separated from Eurasia by the Paleotethys suture. To the south, the Helmand Block is separated from an accretionary prism of Eocene and younger clastic sediments of the Makran Range (McCall, 2002, Figure 1).

The Sistan Suture Zone is a sigmoidal, N-S trending zone that extends from the Neo-Tethys suture to the southk where it is sealed by the Eocene and younger Makran accretionary prism, to a northern termination where the Lut Block and the Helmand Block connect (Figures 1 and 3). The eastern boundary of the suture zone, with the Helmand Block, is covered by Quaternary alluvium that covers all deeper units (Kokaly et al., 2013). The prominent, but inactive, Neogene Hari Rud-Siahan strike-slip fault system is thought to have reworked this eastern boundary (Sargazi et al., 2022; Stöcklin, 1989). To the west of this fault are ophiolites and underlying accreted, partially metamorphosed rocks representing typical ocean plate stratigraphy (OPS) - pillow lavas and other oceanic basement, radiolarian cherts and foreland basin clastics (Isozaki et al., 1990).

Oceanic crustal rocks in the Sistan Suture are commonly all described as 'ophiolite', but comprise both upper-plate-derived, SSZ-type ophiolites and downgoing plate-derived, accreted OPS sequences with a basement showing MORB character (Delavari, 2013). SSZ-type ophiolites are exposed as isolated klippen of a highest structural unit along the eastern side of the suture zone (Karimzadeh et al., 2020; Saccani et al., 2010; Delaloye & Desmons, 1980; Moslempour et al., 2012; Nikbakht et al., 2021). Radiometric ages of the SSZ-type ophiolites are sparse - Delaloyle and Desmons reported a 92 ± 3 Ma K-Ar age, consistent with Turonian pelagic limestones that form the oldest overlying sedimentary cover (Tirrul et al., 1983). The SSZ

spreading phase, typically associated with subduction initiation (e.g., Stern and Bloomer, 1992) is thus thought to be of Late Cretaceous age (e.g., Saccani et al, 2010).
One of the SSZ ophiolites on the eastern side of the suture zone (the Nehbandan Ophiolite) is intruded by leucocratic tonalite, granodiorite, and granite rocks with an arc geochemical signature and a U-Pb zircon age of 58.6 ± 2.1 Ma (Delavari et al., 2014). Similarly, tonalite stocks of the Mahi Rud complex, also with arc magmatic signatures, intrude into pillow lavas that are interbedded with pelagic sediments (Keshtgar et al., 2019). These tonalitic granitoids returned K-Ar amphibole ages of 79.4 ± 3.2 to 83.6 ± 2.6 Ma (Maurizot, 1980; Maurizot et al., 1990) and a recent U/Pb zircon as old as 103.9 ± 2.9 Ma (Bagheri & Damani Gol, 2020).

The ophiolites and their pelagic sedimentary cover are overlain by a more than 8-kilometer-thick Senonian-Eocene turbidite sequence and olistostrome, which reworks ophiolitic rocks as well as shallow-marine derived limestones, and that is interbedded with calc-alkaline volcanic rocks (Camp & Griffis, 1982; Tirrul et al., 1983). This sequence is referred to as the Sefidabeh Basin, which is interpreted as a forearc basin derived from an eastern upper plate that progressed westwards over the accretionary prism (Jentzer et al., 2020; Tirrul et al., 1983; Maurizot, 1980; Fauvelet & Eftekhar-Nezhad, 1990).

Below the ophiolites is an accretionary prism of thin-skinned thrust slices consisting of OPS sequences with westward, and structurally downward decreasing ages of foreland basin clastics, and metamorphic grade suggesting accretion occurred in an E-dipping subduction zone (Angiboust et al., 2013; Delavari, 2013). The structurally highest, and oldest accreted sequence comprises the HP/LT metamorphic Ratuk complex. This consists of metamorphosed and dismembered OPS sequences including metabasalt and -spilite, metacherts, and metaflysch, metamorphosed at eclogite, blueschist, or amphibolite facies (Bonnet et al., 2018; Fotoohi Rad et al., 2005; Kurzawa et al., 2017; Bröcker et al., 2013). Radiolarian cherts gave Cenomanian-Campanian ages, giving a maximum age of metamorphism (Babazadeh & De Wever, 2004). These rocks are mostly exposed as blocks and boulders in a serpentinite mélange thrusted onto a non-metamorphosed mixture of ultramafic and mafic rocks, Cretaceous- Eocene phyllite and Senonian to Maastrichtian pelagic sediments interpreted as OPS sequences of a younger part of the accretionary prism (Agard et al., 2009; Angiboust et al., 2013; Fotoohi Rad et al., 2005). The first mica and amphibole $^{40}Ar/^{39}Ar$ ages of HP metabasites yielded ages between 135 – 125 Ma (Fotoohi Rad et al., 2009) but these data were later explained by contamination with excess Ar

(Bröcker et al., 2013). Instead, ages of HP metamorphism of ~75-86 Ma by Rb-Sr and $^{40}Ar/^{39}Ar$ dating of phengite, white mica, garnet, omphacite, and albite in the blueschist and eclogite, and by ~85-90 Ma U-Pb ages of zircons in the meta-plagiogranite and eclogite are considered to reflect the subduction stage (Bröcker et al., 2013; Kurzawa et al., 2017; Bonnet et al., 2018). To the west, the Ratuk complex thrust onto the Neh complex, which consists of deformed OPS sequences with peridotites and mafic rocks of MORB affinity interpreted as off-scraped material from subducted oceanic lithosphere (Biabangard et al., 2020; Delaloye & Desmons, 1980; Desmons & Beccaluva, 1983; Zarrinkoub et al., 2012). The most prominent mafic-ultramafic unit in this accretionary sequence is the 'Birjand Ophiolite' (Figure 3). Leuco-gabbro yielded zircon U-Pb zircon ages of ~113 ± 1 and 107 ± 1 Ma (Zarrinkoub et al., 2012), and 104.2 ± 0.5 Ma (Bröcker et al., 2022), showing that oceanic spreading in the downgoing plate was still ongoing shortly before or during inception of subduction. Radiolarian red clay-rich pelagic sedimentary rocks in the OPS units in the south of the Neh complex returned ages as old as the Albian-Aptian (~120-100 Ma) (Ozsvárt et al., 2020), and foreland basin clastics give ages ranging from Upper Cretaceous to the lower Eocene ages marking the arrival in the trench (Tirrul et al., 1983). The Neh Complex is mostly non-metamorphic, rare mica schists yielded white mica ages of 68 ± 3.0 Ma and 65 ± 2.0 Ma (K-Ar method) (Delaloye & Desmons, 1980). Collectively, these relationships suggest that oceanic spreading of the subducted ocean floor continued until at least ~104 Ma, that eastward (in modern coordinates) subduction in the Sistan subduction zone was underway by 90 Ma, and perhaps 103 Ma (corresponding to the oldest ages found in the Mahi Rud arc-related plutons), and that subduction ceased in the mid-Eocene. All units of the Sistan Suture Zone, as well as the neightboring continents were regionally unconformably covered by upper Eocene shallow-water nummulitic limestone (Eftekhar-Nezhad & Stöcklin, 1992; Gholami et al., 2015), and red beds (Rowshanravan et al., 2006), Oligocene and younger volcanic rocks (Tirrul et al., 1980; Pang et al., 2012). These magmatic rocks are interpreted to originate from the post-collisional processes such as crustal delamination following the arrest of subduction between the Lut and Helmand blocks (Pang et al., 2013 Bagheri and Damani Gol, 2020). After the middle Eocene, the Sistan Suture was deformed along N-S trending strike-slip faults, including the Hari Rud Fault and the prominent Neh Fault system (Figure 1) with dextral displacements of some tens of kilometers (Stöcklin, 1968; Walker & Jackson, 2004).

Thick Oligocene and younger volcanic and volcano-sedimentary series also covers much of the pre-Eocene geology of the northern termination of the Sistan Suture Zone (Figure 4). Exposures in erosional windows below this young volcano-sedimentary cover show that the Ratuk complex, Neh complex, and Sefidabeh basin curve in the north of the suture zone into a NW trend (Figure 3). The northeasternmost exposed parts of the Ratuk complex forms a narrow NW trending belt of mélange of Cretaceous ultrabasic rocks and red pelagic sediments and turbidites (Fauvelet & Eftekhar-Nezhad, 1990). The northernmost outcrop of the Ratuk complex is overthrust in the east by what we here call the Afin Belt that we infer to be part of the Helmand Block. This consists of Jurassic intermediate volcanic, volcano-sedimentary and intrusive rocks overlain by upper Cretaceous-Paleocene shallow-marine limestones, deformed by NW-SE trending folds and thrusts (Fauvelet & Eftekhar-Nezhad, 1990) (Figure 3).

The Sistan Suture Zone units as well as the Afin Belt are abruptly cut to the NW by a NE-SW-trending curvilinear fault zone and adjacent fold-thrust belt that trends perpendicular to the trend of the Sistan Suture Zone units. To the northwest of this termination are Paleozoic rocks and Jurassic magmatic-metamorphic rocks of the ‘Qaen (Qayen) Allochtonous Belt’ (Bagheri and Damani Gol, 2020) that are contiguous with the Lut Block (Bröcker et al., 2014; Bagheri and Damani Gol, 2020).

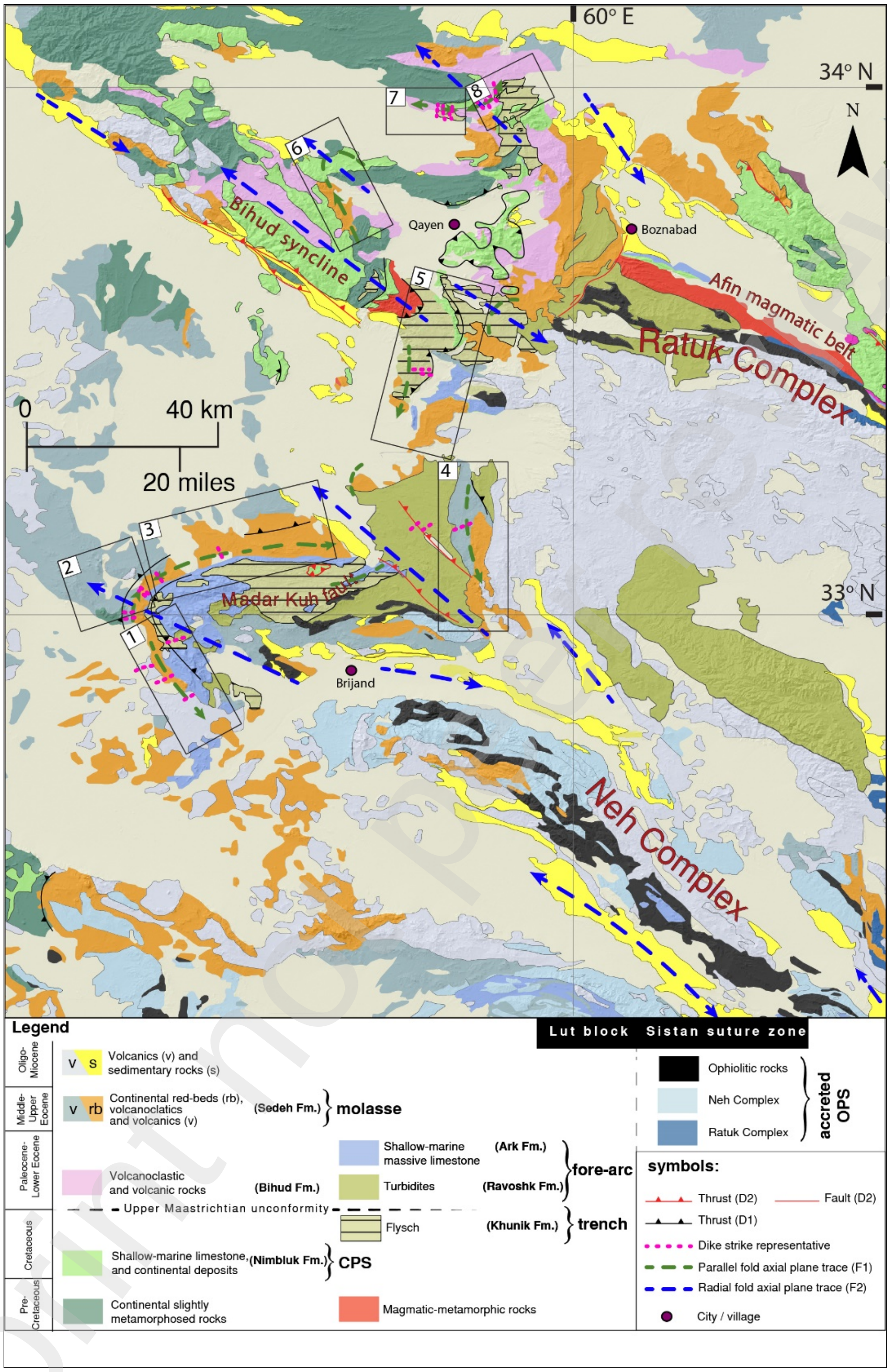

Figure 4. Geological map of the northern termination of the Sistan Suture Zone. Representative strikes of fold axial planes are indicated for both radial folds/F2 in blue dashed lines and parallel folds/F1 in dark green dashed lines. Pink dotted lines represent the strike of dikes that cut across the F1 folds. The curved belt is divided into eight segments (1-8), numbered from Khusf area in southwest to Achāni area in northeast of the belt.

3. Results

3.1. Stratigraphy

The north(west)ern termination of the Sistan Suture Zone is well reflected in the stratigraphic units that occur around its margin, with contrasting pre-Eocene lithologies (Figure 4). The margin of the Lut Block adjacent to the northern termination of the Sistan Suture Zone contains a stratigraphy comprising continental and shallow open marine sediments from Paleozoic to the upper Cretaceous (Fauvelet & Eftekhar-Nezhad, 1990). The uppermost of these is the Nimbluk Formation that consists of shallow marine limestones and near-shore terrestrial deposits (Figure 4). The Numbluk Formation is overlain by the Bihud Formation that covers a vast area to the north of Qayen and comprises basic to intermediate volcanics, interfingering with detrital and volcaniclastic sediments with interlayers of lacustrine limestone, deposited in a non-marine environment. These volcanics and sediments have not been dated but the age of the basal layers of their unconformable cover have been dated as early Eocene (Fauvelet & Eftekhar-Nezhad, 1990).

Towards the suture zone, deeper-marine rocks are exposed interpreted as the margin between the Lut Block and the deep-marine flysches of the Sistan Suture Zone. Notably, these comprise Turonian-Maastrichtian green shales, yellowish Orbitholina-bearing sandstones, sandy limestones with intraformational conglomerates, and scarce, massive limestone layers collectively known as the Khunik Flysch Formation (Fauvelet & Eftekhar-Nezhad, 1990). Boulders and olistoliths of limestone are locally included within the shales ("wild flysch"). The Khunik Flysch Formation occupies an extensive northeast-trending belt, from ~65 km west of Birjand city towards the Afin Belt (Figure 4). The Khunik Flysch Formation is interpreted to be deposited in a deep, narrow basin, and was at least in part derived from the adjacent Lut Block as it also unconformably covers folded Jurassic and Lower Cretaceous limestones of the Lut Block margin to the north (Fauvelet and Eftekhar-Nezhad, 1990). The Khunik Flysch Formation is unconformably overlain by the Ravoshk Formation that crops out along a NE-trending 80-km long belt from west of the Birjand to Boznabad (Figure 4). It comprises turbiditic sandstones, calcareous shale, conglomerate, and sandy limestone ranging in age from the upper Maastrichtian to the Paleocene and lower Eocene. Besides the Khunik Flysch Formation, the Ravoshk Formation also covers ultramafic rocks and metamorphic rocks of the Ratuk and Neh Complexes. To the north of Birjand, the Ravoshk Formation is unconformably overlain by the Ark Formation that consists of basal red conglomerates overlain by shallow-marine massive nummulitic limestone and marls and marly limestones of the Paleocene-lower Eocene. This limestone is interpreted as deposited in a southeastward deepening open, shallow marine environment.

The middle Eocene and younger stratigraphy that covers both the Sistan Suture Zone and the Lut Block stratigraphy is the non-marine Sedeh formation, whose thickness exceeds 2000 meters. Two intercalated main depositional units red-beds and andesitic pyroclastic deposits and lavas. These volcanic rocks are regionally associated with dikes that cut the deeper stratigraphic units and that are not observed to cut the Oligocene-Pliocene rock units. The Sedeh Formation unconformably overlies older formations, with a widely recognized basal conglomerate. The formation is thought to have been deposited in playas and lakes in a volcanically active environment (Fauvelet & Eftekhar-Nezhad, 1990). Extensive Oligocene-Pliocene volcanic and sedimentary rocks unconformably overlie all former formations in a vast area of the north of the Sistan Suture (Fauvelet & Eftekhar-Nezhad, 1990).

3.2. Structure

3.2.1. Madar-Kuh Fault

The metamorphosed, folded, and thrusted rocks of the Neh and Ratuk accretionary complexes abruptly terminate against a curvilinear fault that is roughly perpendicular to the trend of the Sistan Suture Zone (Figure 4). We identify this curvilinear fault as the Madar-Kuh Fault, which is currently a thrust fault placing the Khunik Flysch and older rock units of the southeastern Lut margin over rocks of the Sistan Accretionary Complex (Figure 5). The Madar-Kuh Fault is in most places covered by alluvium or Oligocene-Pliocene volcano-sedimentary rocks, but where it is exposed, it places the Khunik Flysch over peridotite slices of the deformed and uplifted OPS of the Neh complex (Figure 5). Twards the northeast, south of Qayen (Figure 3 and 4), the Khunik Flysch Formation thrusted onto the Ratuk complex and overlying ophiolites (Figure 6). The Madar-Kuh Fault is dipping to the northwest suggesting a southeastward thrust direction, although an oblique component cannot be excluded.

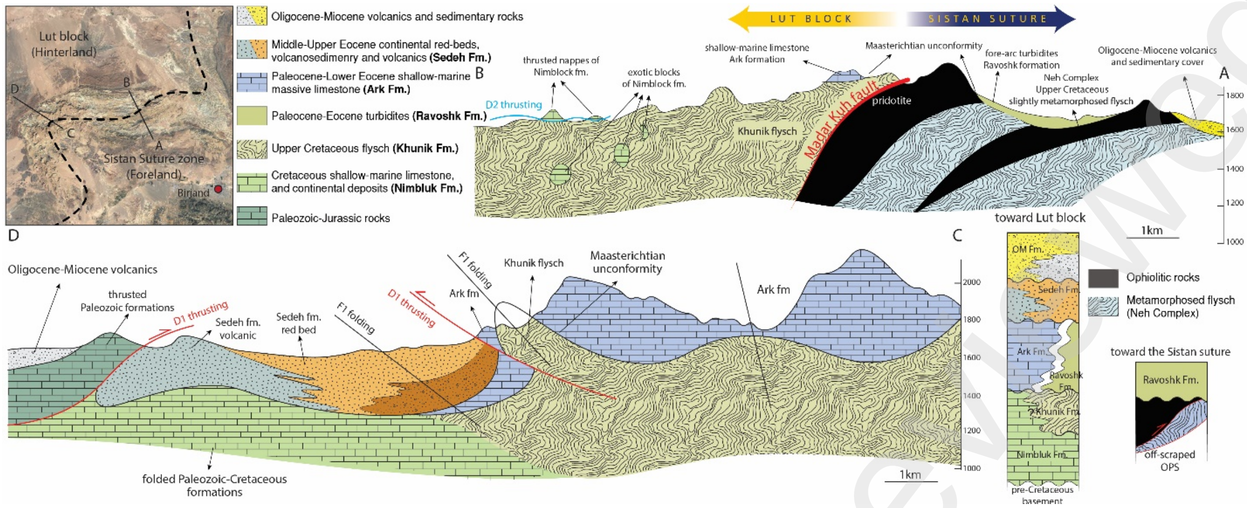

Figure 5. Cross-sections and stratigraphic columns of the northwestern termination of the Sistan Suture Zone, displaying the thrusting of the deformed Lut Block margin onto the Neh complex in the Birjand area; Cross section A-B displays the steep Madar-Kuh Thrust that places the Khunik Flysch Formation onto deformed and uplifted OPS units of the Neh complex. Cross section C-D displays the shortening affecting formations of up to Eocene in age at the southeastern margin of the Lut Block. The stratigraphic columns display the stratigraphic relationships and disconformities in the Sistan and Lut domains.

The southeastern margin of the Lut Block in the hangingwall of the Madar-Kuh Fault has been deformed in a narrow belt of approximately 20 km wide that displays two phases of deformation. The older consists of thrusts and associated folds that trend parallel to the curvilinear Madar-Kuh Fault. For instance, South of Qayen, shallow-marine Cretaceous limestones of the Nimbluk Formation were thrusted southeastward onto the Khunik Flysch behind the Madar-Kuh Fault that placed the Khunik Flysch Formation onto the Ratuk complex (Figure 3 and 6). Towards the southwest, section C-D of Figure 5 shows how the Paleozoic to Jurassic stratigraphic units of the Lut Block, as well as the Paleocene-Eocene Ark Formation are folded, and thrusted over the lower-middle Eocene Sedeh Formation, both southeastward as well as backthrusted northwestward. These folds and thrusts are parallel to and deform the hanging wall of the Madar-Kuh Fault. Mesoscale recumbent isoclinal folds are located close to thrust contacts (Figure 7). These overall NE-SW trending first-generation folds and thrusts were previously referred to as ‘parallel folds’ by Bagheri and Gol (2020). The youngest formation that we observed to be affected by this first-generation ‘parallel’ folding is the lower to middle Eocene Sedeh Formation.

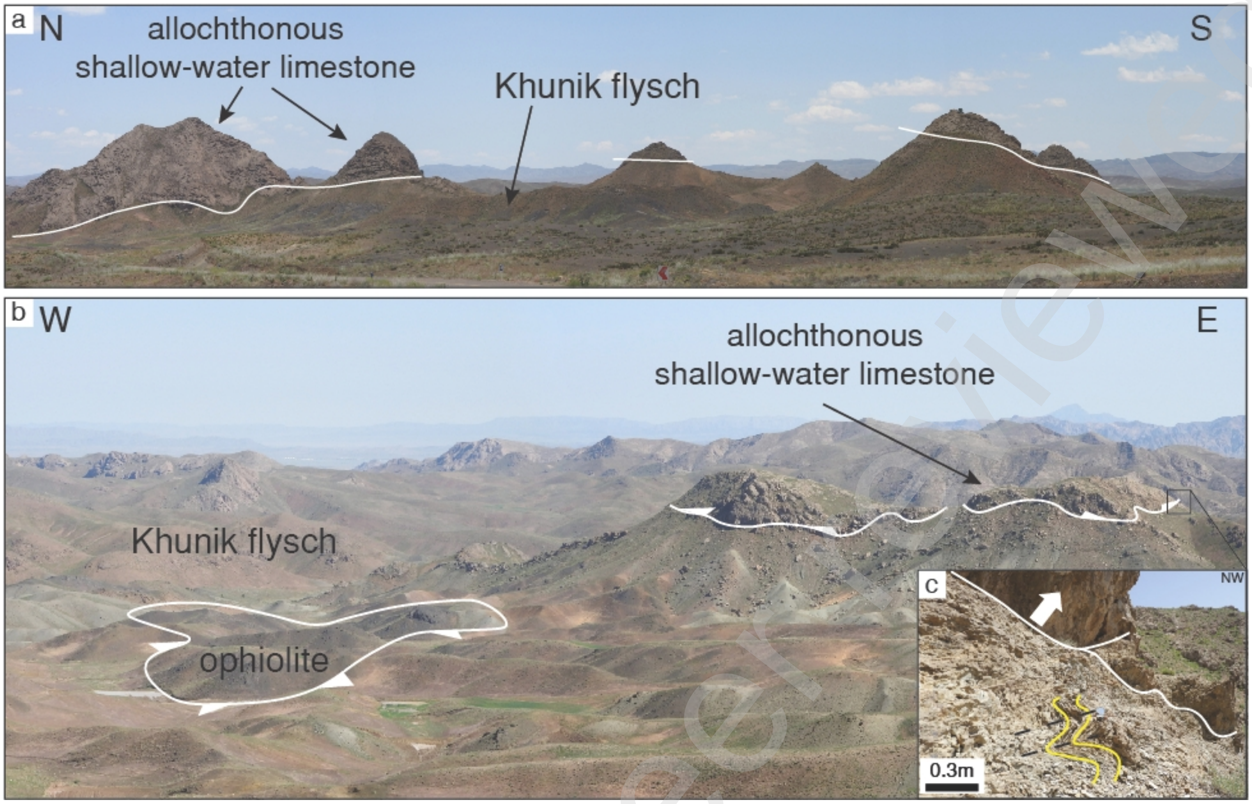

Figure 6. Panoramic views of the Nimbluk Formation allochthonous bodies, that belong to the Lut Block shelf, thrusted upon the Khunik Flysch Formation that belongs to the margin towards the Sistan Suture Zone. (a & b), (c) a close-up of the tight folds within the Khunik Flysch Formation close to the contact.

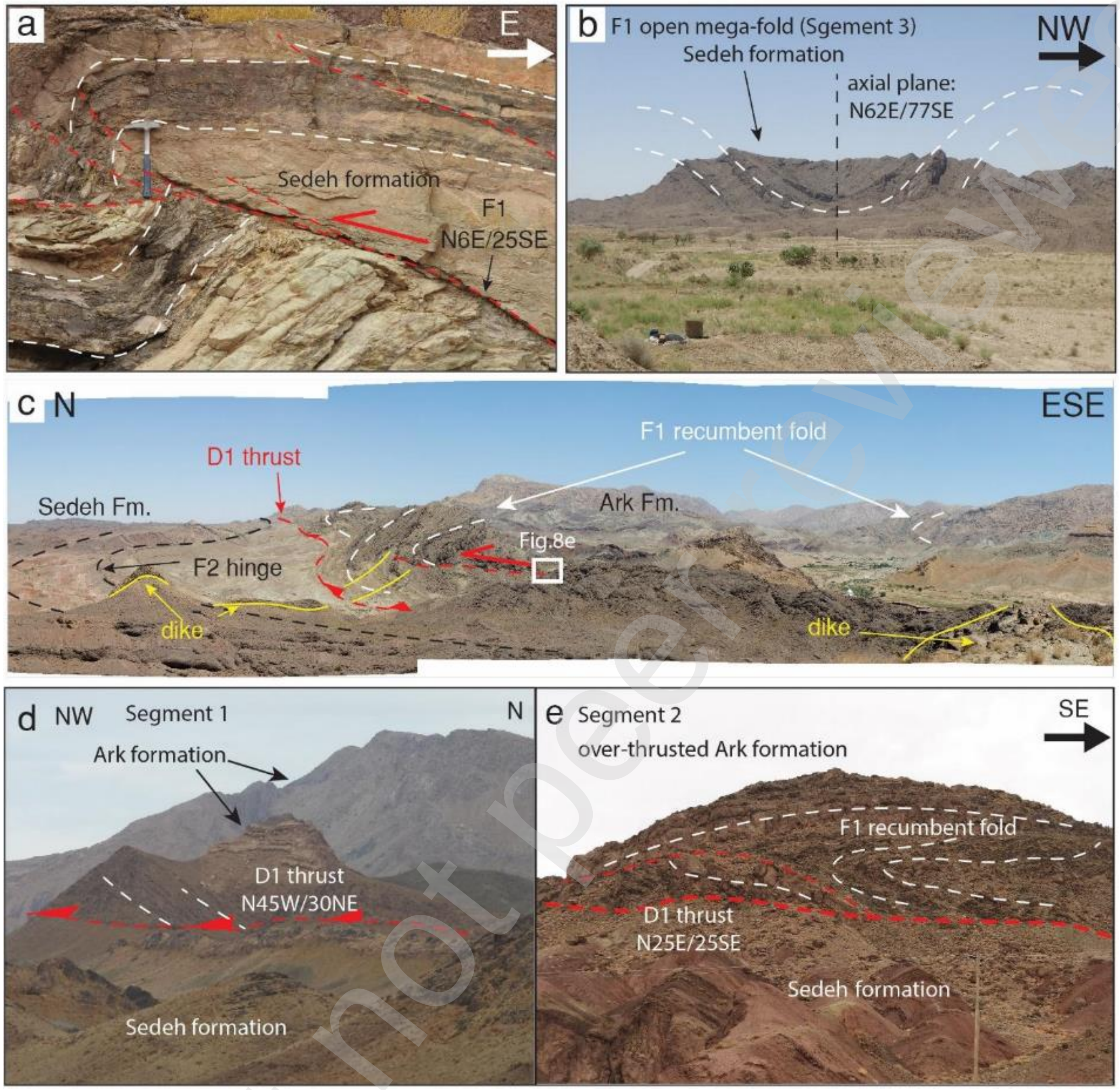

Figure 7. Photographs of key field relationships, (a) a thrust surface within the middle Eocene Sedeh Formation (Segment 2, Figure 3); (b) open parallel F1 folds in the Sedeh Formation on the southeastern margin of the Lut block (c), landscape view of post-middle Eocene thrusting (D1) with recumbent folds in the hanging-wall. Dikes form cut the flanks of the F1 folds and form a fanning pattern as the F1 folds are refolded by F2 folds with fold axial planes roughly perpendicular to the F1 fold; (d, e) thrust faulting (D1) of Ark Formation onto the Sedeh formation.

The first-generation folds and thrusts were refolded by smaller-scale folds with fold axes that trend near-perpendicular to the F1 folds, i.e., NW-SE. Refolding results in plunging antiforms and synforms where F2 folds refold dipping F1 fold limbs. This second generation of folds was previously referred to as 'radial folds' by Bagheri and Gol (2020). Our structural observations show that Oligocene to even Pliocene rocks are affected by this second generation folding

(Figure 8), but these post-Eocene rocks display no evidence for the first-generation folding. We infer that the curvilinear trace of the Madar-Kuh Fault at the northern termination of the Sistan Suture Zone, is the result of the interference of the two generations of folding (and thrusting) that affected the northwestern Lut-Sistan margin after the early to middle Eocene.

Along the strike of the hanging wall of the Madar-Kuh Fault, the F1 folds are cut by swarms of monzodioritic dikes (Abbakhsh et al., 2018). The dikes vary in width from 1 to 30m and are typically 6-8m wide and exposed lengths are at least some 200 m. The dikes cut through all formations up to the Eocene Sedeh Formation, but we did not observe them in younger formations.

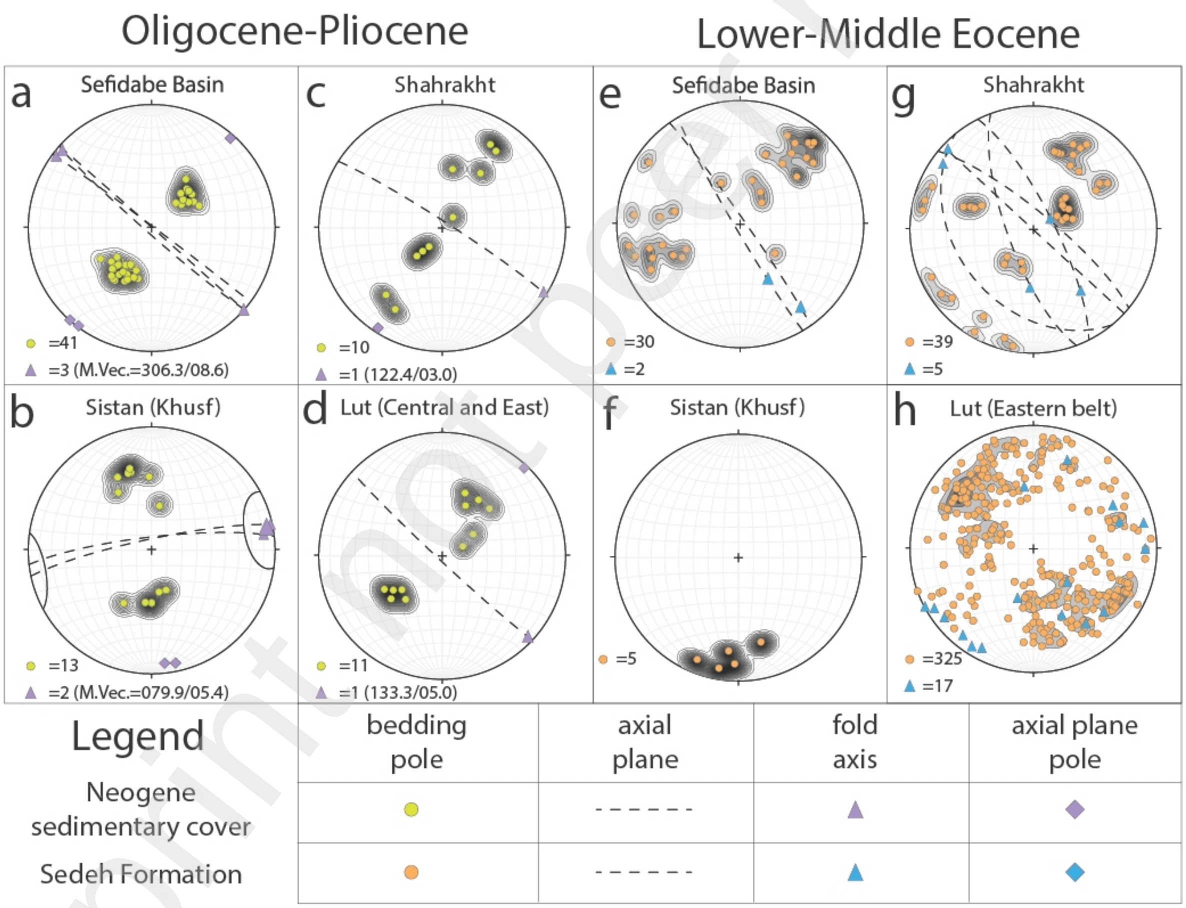

Figure 8. Southern hemisphere equal-area projection of bedding of Neogene sedimentary cover and the middle Eocene red beds (Sedeh Formation) of the Sistan Suture Zone and the Lut Block. Folding analysis of the Neogene of the Sefidabeh basin (a) comparing to west of the Sistan Suture, Khusf region (b), the northeast of the suture, the Esfand region (c), and other regions of the Lut Block (eastern belt and central Lut) (d); fold analysis of the F1 folds from Sedeh Formation of the Sefidabeh basin with open folds by NW-SE upright axial plane (e); northeast of the suture, the Esfand region by folds with NW-SE axial plane strike, occasionally recumbent folds (g); west of the Sistan suture, the Khusf region (f) adjacent to the eastern belt of the Lut

Block (h). Note the data of the F1 folds on the curved belt does not represent a unique and simple orientation of the folding axial planes, as a result of second generation F2 folding.

The dikes trend near-perpendicular to the F1 fold axes and this angular remains consistent despite the curvilinear shape of the F1 folds due to F2 refolding. The dikes as a result define a fanning pattern (Figure 9 a and c). A clearly positive orocline test (Pastor-Galan et al., 2017) between the dike strike and the bedding strike of the cross-cut F1 fold limb, measured along the length of the Madar-Kuh hanging wall quantitatively demonstrates that the fanning of the dikes is straightforwardly explained by F2 folding. From this, we infer that the dikes intruded after F1 and prior to F2 folding (Figure 10). Two dike samples from the north and the south of the study area were collected for U-Pb zircon dating to constrain the minimum age for the first folding and the maximum age for the second folding phase.

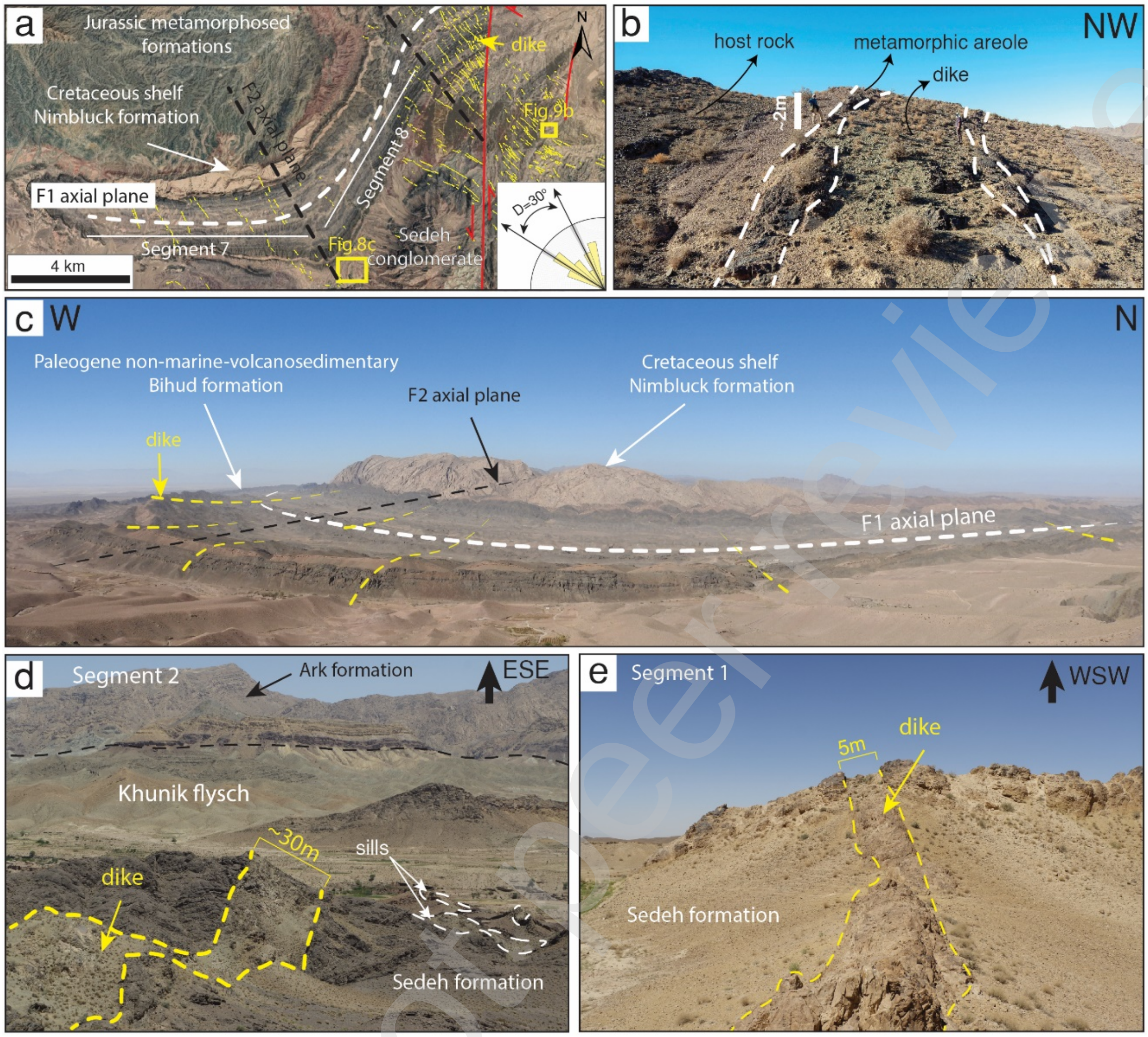

Figure 9. Photographs of key field relationships on the curved belt along the Madar-Kuh Fault that forms the northwestern termination of the Sistan Suture Zone: (a) Google Earth image of a dike swarm that orthogonally cuts the axial plane of the F1 Achāni syncline, (b) a single ~6-meter-thick andesitic dike intruded within the Paleocene-Eocene Bihud Formation volcano-sedimentary rocks, with the baked-contact metamorphic areole; (c) panorama from the southern convex of the Achāni structure and plotted dikes (yellow dash line) cut through the curved F1 axial plane (white dashed line) that is folded around the F2 axial plane (black dashed line), (d) a E-W striking, 30-meter thick andesitic dike intruded within the Sedeh red-beds at the segment 3 (see Figure 3), and (e) a post-middle Eocene dike cutting the Sedeh Formation at the segment 1 (see Figure 3).

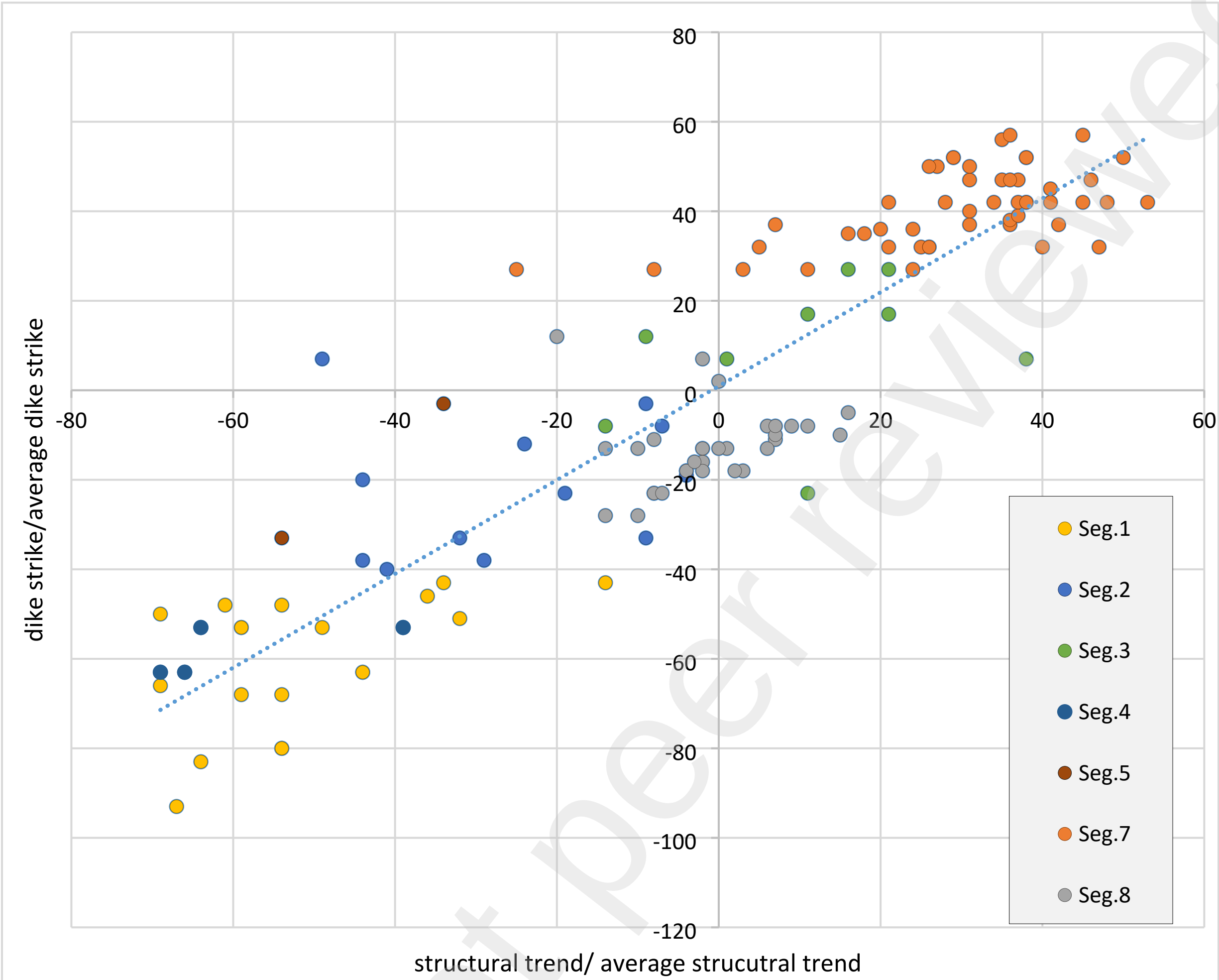

Figure 10. Orocline test (Pastor-Galan et al., 2017) showing a systematic angular relationship between the strike of F1 fold limbs and the strike of cross-cutting dikes. This suggests that the dikes intruded after F1 but prior to F2 folding.

4. Dating of dikes

Zircon grains were separated from ~5 kg rock samples by conventional heavy liquid and magnetic techniques, and then picked by hand under a binocular microscope. For all samples, more than 150 zircon grains were randomly selected from over 500 grains, mounted in epoxy resin, and polished to expose the inner part of the zircon grains. Transmitted and reflected light were used to avoid cracks and inclusions, and cathodoluminescence (CL) images, obtained by a CAMECA electron microscope, were used to identify the morphology and internal texture of the zircon grains.

Zircon U-Pb age analyses were performed by using an Agilent 7500a ICP-MS equipped with a 193-nm laser ablation system at the Institute of Geology and Geophysics, Chinese Academy of Sciences (IGGCAS). Analytical procedures followed the method described in Wu et al. (2010). For each sample, at least 30 zircon grains were dated with a spot diameter of 32 μm. The standard zircons (91500 and GJ-1) were used to determine the U-Th-Pb ratios and absolute elemental concentrations of the analyzed zircon. Data were processed with the GLITTER program (Griffin et al., 2008). The $^{206}Pb/^{238}U$ ages are used for zircons with concordant ages less than 1,100 Ma, and $^{207}Pb/^{206}Pb$ ages are used for zircons when $^{206}Pb/^{238}U$ ages are older than 1,100 Ma. A data plot was conducted by using the Density Plotter program (Vermeesch, 2012). Only the youngest ages from the rim of the zircon crystals were employed as the emplacement age of the monzodioritic dikes. All the U-Pb data are provided in Supplementary Table 1.

Forty-five zircon grains were measured from sample ACH-401 from the northeast end of the parallel fold, 16 zircons yield a concordant $^{206}Pb/^{238}U$ age at 43.1 ± 0.5 Ma (1σ, n = 28, Figure 11). For Sample DR-5b that was collected from the southwestern end of the F1 fold system, individual data points are scattered, ranging from the late Eocene to the Mesoproterozoic suggesting the presence of xenocrysts. The youngest cluster consists of 6 zircons (30 analysis) that yield a concordant $^{206}Pb/^{238}U$ age of 51.3 ± 1.5 Ma (1σ, n = 6, Figure 11), that we interpret as the dike crystallization age.

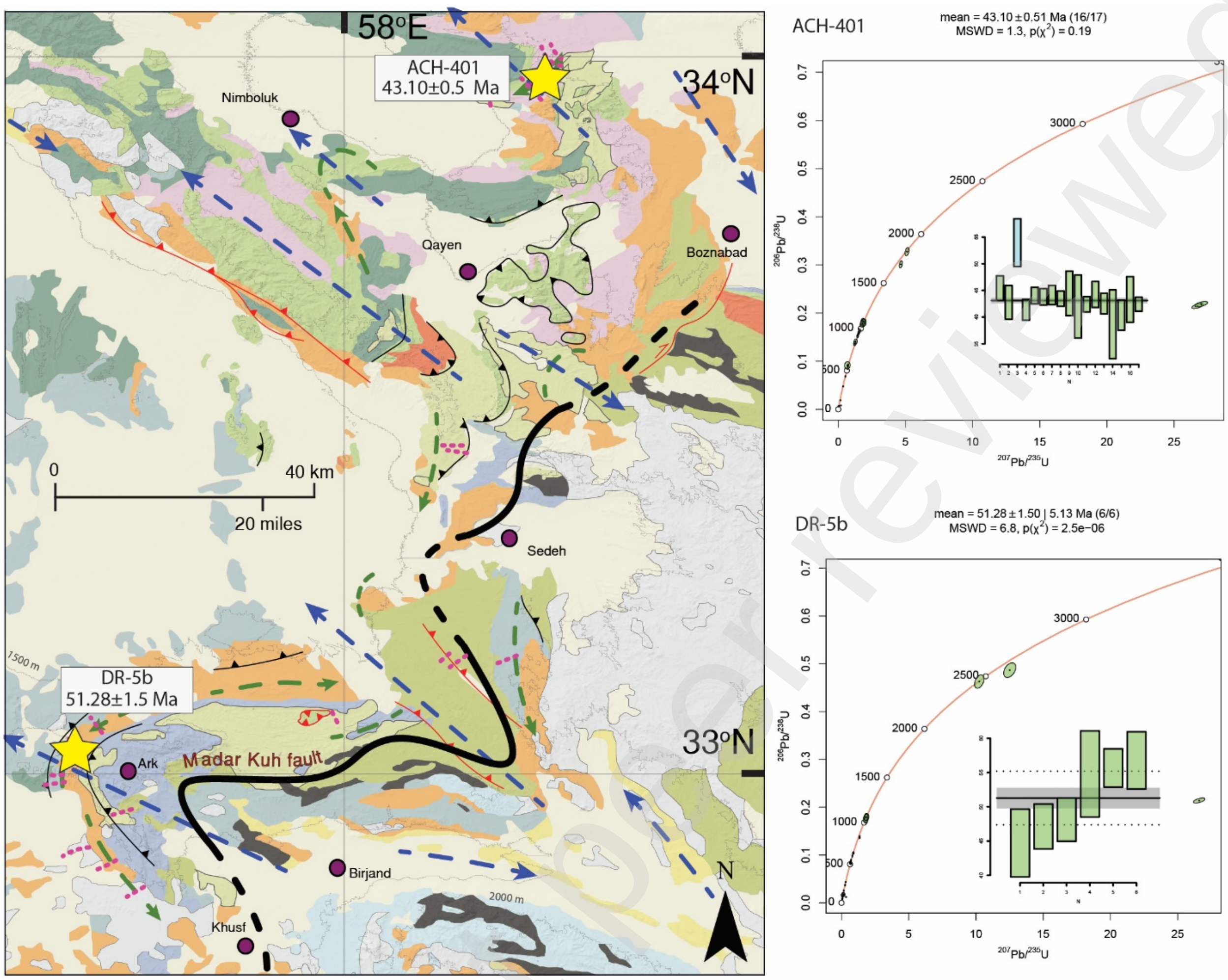

Figure 11. Results of isotopic U-Pb dating of zircon crystals obtained from the dikes that cut F1 folds and were folded by F2 folds. For the legend of the geological map, see Figure 4.

5. Discussion

The abrupt northern termination of the Sistan Suture Zone was previously tentatively interpreted by Bagheri and Damani Gol (2020) as the result of tight oroclinal buckling. This hypothesis invoked that the Sistan Suture Zone curves 180° in the north and is surrounded by the Lut Block (Figures 2a and 12). This interpretation predicts that the Ratuk complex is also present on the western side of the suture zone along the eastern margin of the Lut Block. However, no HP-LT metamorphic rocks have so far been discovered at the eastern margin of the Lut Block.

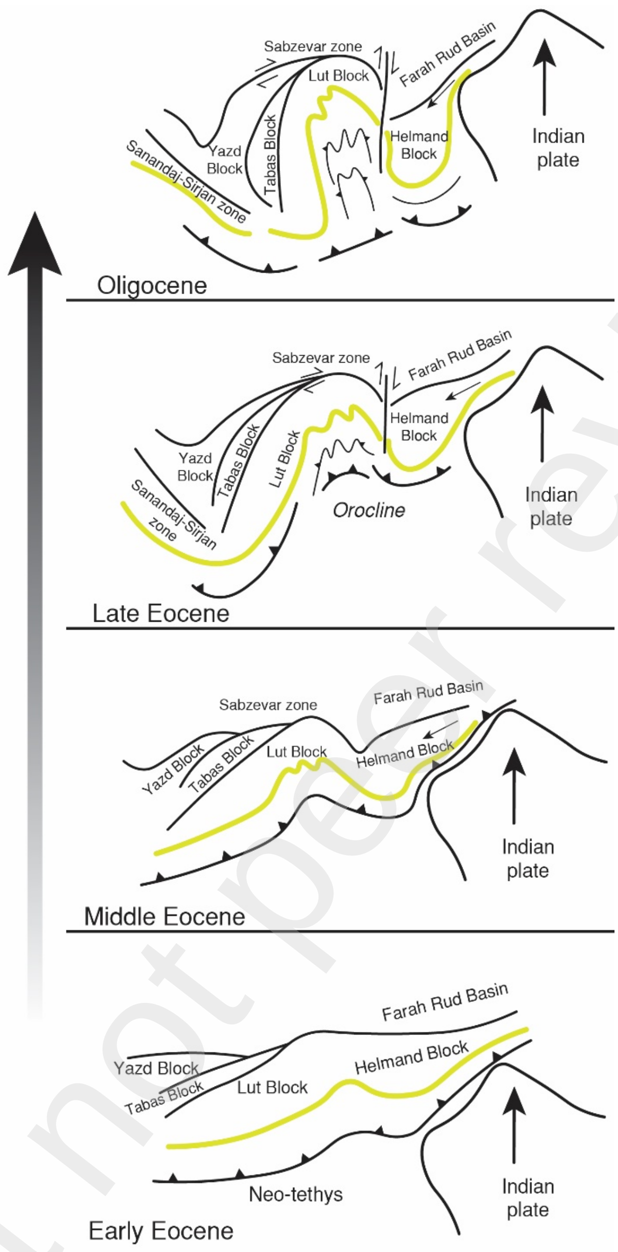

Figure 12. Cartoons illustrating how E-W shortening occurred in eastern Iran due to the westward extrusion of the Helmand Block away from the Tibetan orogen. The green line represents deliniates the southern margin of the Cimmerian blocks under the hypothesis of Bagheri and Damani Gol (2020) that the Sistan Suture Zone would represent a northward convex orocline.

In contrast, our analysis shows that the Madar-Kuh Fault zone forms an abrupt northern ending of the 750 km long, N(W)-S(E) striking Sistan Suture Zone. Our new structural data show that in its modern orientation, the Madar-Kuh Fault Zone is a SE-verging thrust that places shallow-marine rocks and volcanics correlated to the Lut Block, with ages up to the Eocene, over deformed rocks of the Sistan Suture Zone accretionary prism and that in the hanging wall of this fault is a series of parallel folds and thrusts of the same age. The curvilinear Madar-Kuh Fault and associated fold-thrust belt terminate where also the Sistan Suture Zone terminates in the southwest. In other words, this fault appears to be related to the formation of the suture zone, rather than representing an unrelated younger fault system. Moreover, our study shows that the curvilinear nature of the fault zone reflects a second folding phase that accommodated some shortening roughly parallel to the Madar-Kuh Fault Zone and that caused the curvilinear shapes by fold interference. The U-Pb zircon ages of andesitic dikes affected by the second, but not by the first folding phase, as well as the biostratigraphic ages of the folded strata show that the second phase of folding postdates the 43.1±0.5 Ma intrusion of the youngest dated dike, and hence post-dates the arrest of formation of the accretionary prism, and subduction, in the Sistan Suture Zone. The first folding, and the associated southeastward thrusting of the Lut Block over the northwestward termination of the Sistan Suture Zone occurred after the deposition of the Paleocene to lower Eocene Ark formation and prior to the 51.2 ± 1.5 Ma intrusion of the oldest dated dike cutting the F1 fold. From this, we infer that the thrusting along the Madar-Kuh Fault occurred in the latest stages of, or just after its final closure and the arrest of subduction in the Sistan Suture.

In other words, the Madar-Kuh Fault, was a straight fault during the formation of the Sistan Suture Zone, striking perpendicular to the suture zone, and without a demonstrable vertical component, but with continental crust overlain by shallow marine to non-marine deposits on the north(west)ern side, and deep-marine, oceanic rocks on the south(east)ern side. The eastward subduction of the Sistan ocean below the Helmand Block from the Late Cretaceous to the Eocene must have been associated with major E-W convergence, during which the Helmand Block advanced towards Iran and the Sistan Suture Zone retreated towards the Lut Block. The total amount of convergence is difficult to estimate from only our field observations and requires regional kinematic restoration, but given that subduction and accretion spanned at least some 40 Ma, from ~90-50 Ma, at least some hundreds of kilometers of subduction seems a reasonable estimate. The only tectonic way in which a subduction zone can end abruptly is through a transform fault, or, more specifically, a subduction transform edge propagator (STEP) fault (Figure 13), which becomes younger (i.e., propagates) in the direction of the downgoing plate, as subduction progresses (Govers & Wortel, 2005). We infer that the Madar-Kuh Fault must represent the youngest portion of the STEP fault that accommodated the westward westward retreat of the Sistan Subduction Zone towards the Lut Block ahead of the extruding Helmand Block away from an original position within the western Tibetan/Karakoram orogen. This inference of large-scale extrusion echoes the conclusions of Bagheri and Damani Gol (2020) and Şengör et al. (2023) (Figure 13). iven the overall N-S strike of the Sistan Suture Zone, we infer that the curvature to NW-SE at its northern termination, as well as the NE-SW strike of the Madar-Kuh Fault result from counterclockwise vertical axis rotation that is well-documented from the Lut Block (Mattei et al. 2012, 2015; Soffel et al. 1996), and that the original orientations were ~N-S and E-W, respectively. We speculate that the eastward continuation of this STEP fault is the Waser (Waras-Panjaw) suture zone between the Helmand Block and the Farah Rud Basin of Afghanistan (Boulin, 1990; Girardeau et al. 1989; Şengör 1984; Stöcklin, 1989, Tapponier et al. 1981) (Figure 13).The well-documented N-S Neogene shortening in the Kopet Dagh thrust belt of NE Iran (Hollingsworth et al. 2010; Lybéris and Manby, 1999) must have displaced the Madar-Kuh Fault and Sistan Suture Zone northward relative to the Afghan orogenic infrastructure, but future detailed restoration of the Iranian-Afghan orogen is required to further evaluate this hypothesis.

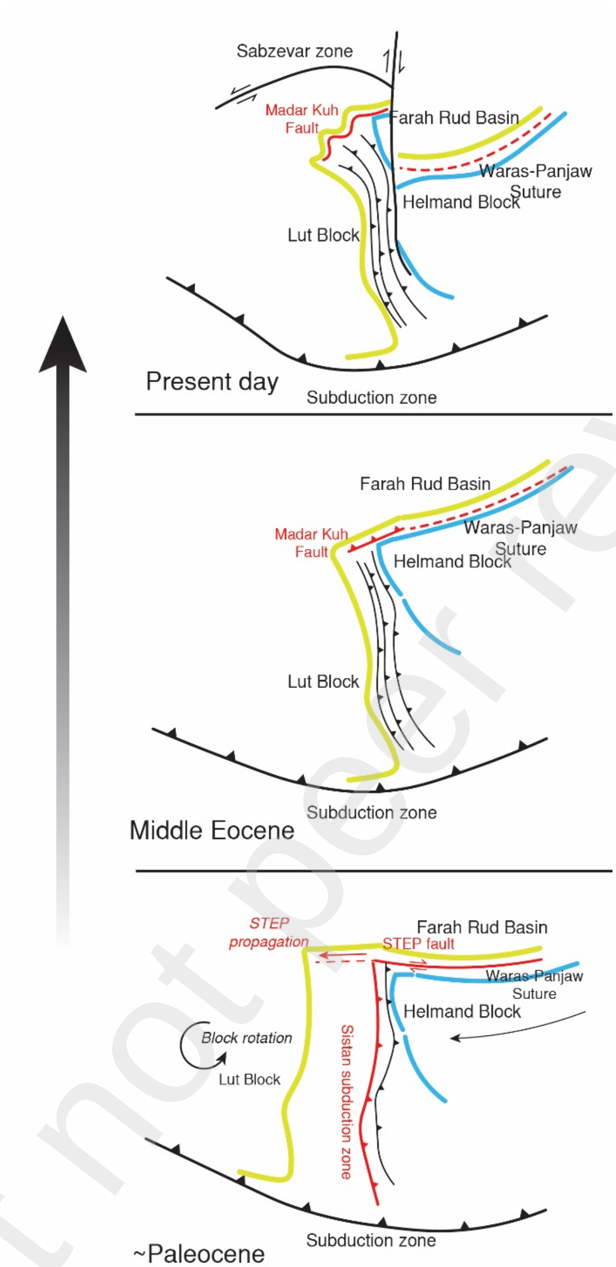

Figure 13. Cartoons illustrating the evolution of the Madar-Kuh Fault at the northern termination of the Sistan Suture Zone as a late-stage STEP fault that propagated from the east during the advance of the Helmand Block that led to the subduction and closure of the Sistan Ocean. Green line represents the passive margin of the Lut block), the blue line outlines the margins of the Helmand Block, and the red line shows the western and northern plate boundary that represents the subduction zone consuming the Sistan ocean, and the STEP fault that connects this trench to the east and accommodated Helmand Block extrusion to the west.

Our data suggest that the Madar-Kuh STEP fault formed along the transition between the Sistan Ocean basin and continental crust of the Lut Block that bounded the ocean to the north. This suggests that the Lut Block had a ~90° kink in its passive margin, which likely represents an older transform fault inherited from its rifting and opening history. Such formation of a STEP fault along a continent-ocean boundary may for instance be comparable to the Miocene STEP fault along the north African margin of Algeria and Morocco that formed during the westward retreat of the Gibraltar slab (Govers and Wortel, 2005; Spakman and Wortel, 2004; van Hinsbergen et al., 2014). The ongoing N-S convergence between Africa and Europe there led to inversion of this STEP fault as a presently active thrust system (Deverchere et al., 2005; Baes et al., 2011). This inversion may form an analogy for the Madar-Kuh thrusting over the Sistan Suture Zone in the latest stages of, or just after subduction and STEP fault propagation.

Its abrupt termination at the Madar-Kuh Fault shows that the Sistan Suture Zone is not contiguous with the isolated remains of the Sabzevar Suture Zone of northern Iran, as sometimes hypothesized (Bröcker et al. 2022; Rossetti et al. 2010). Instead, the Sabzevar suture zone is likely genetically linked to the Nain-Baft, or Inner Zagros suture zone, offset along the large-displacement Great Kavir Fault that also displaced rocks from the Paleo-Tethys suture zone into Central Iran (Bagheri and Stampfli, 2008). The Sistan Suture Zone was not the only location of long-lived subduction in Central Iran, and pre-mid Cretaceous paleogeography of the Iranian-Afghan realm must thus have been vastly different from today's.

Finally, the long-lasting subduction episode that closed the Sistan Ocean, starting at or before ~90 Ma (Bröcker et al., 2013) and lasting until the Eocene, ~50 Ma has important regional implications for the geodynamic evolution of both the tectonic construction and evolution of the Iranian Plateau as well as the western Tibetan/Pamir Plateau. Although based on the information from the Sistan Suture Zone alone it is not possible to estimate the total amount of subduction involved, the ~E-W convergence that drove its closure requires that the Helmand Block in the hanging wall of the Sistan subduction zone restores far east- or northeastward of its present-day location. This suggests that the Helmand Block was part of one of the continental tectonic terranes that are identified in the Pamir-Hindu Kush region, and which correlate to the continental fragments that constitute the Tibetan Plateau (Robinson, 2015). Our identification of the northern termination of the Sistan Suture Zone as a STEP fault will aid the reconstruction of the still-enigmatic westward extrusion tectonics from the west-Tibetan orogenic collage, and the associated subduction that closed the Iranian back-arc basins in Cretaceous to Eocene time (Figure 13).

6. Conclusion

In this paper, we study the tectonic history of the abrupt northern termination of the Sistan Suture Zone that formed during late Cretaceous to early Eocene subduction in eastern Iran between the continental Lut Block of central Iran and the Helmand Block of Afghanistan, both located in the upper plate of the Neo-Tethyan subduction system. We show that the westward younging, ocean-derived Sistan accretionary prism continues to a sharp boundary formed by the Madar-Kuh thrust fault that emplaced continental margin rocks that correlate with the Lut Block over the accretionary prism. The Madar-Kuh fault is curvilinear in nature, strikes nearly perpendicular to the overall strike of the Sistan Accretionary Prism, and is associated with D1 folds and thrusts in its hanging wall that strike parallel to the main thrust. The Madar-Kuh fault disappears southwestwards where also the Sistan Accretionary Prism disappears, but continues northeastward beyond the suture zone, between rocks correlated to the Lut and the Helmand blocks. From this we infer that the Madar-Kuh fault is genetically related to Sistan Ocean closure, and not to an unrelated later deformation phase.

We show that the curvilinear nature of the Madar-Kuh fault results from younger refolding. The Monzodioritic dikes that cut the first-phase folds and that were folded by the second were dated at 51.3±1.5 Ma and 43.1±0.5 Ma, showing that the second folding occurred well after Sistan Ocean closure. The first folding phase and thrusting along the Madar-Kuh Fault occurred in the waning stages of Sistan ocean closure. During Sistan ocean subduction, the Madar-Kuh Fault thus formed a trench-perpendicular, abrupt termination of the subduction zone. We interpret it a STEP-fault connected to an east-dipping subduction zone that accommodated the advance of the Helmand Block towards the Lut Block. We speculate that this STEP fault continues as the Waser suture zone between the Helmand and Farah-Rud blocks of Afghanistan. This overall ~E-W convergence must have involved extrusion of the Helmand Block away from the western Tibetan/Pamir orogen, into the Iranian back-arc basins. Recognizing that the Sistan Suture Zone abruptly ended at a STEP fault provides a kinematic clue towards reconstructing this extrusion history, which will impact the understanding of the dynamics and paleogeography of the Tibetan and Iranian plateaus alike.

Acknowledgments

This work was supported by the research project of Ferdowsi University of Mashhad, Mashhad, Iran (no. 48315), and National Natural Science Foundation of China (no. 42261144673) to S. Li. NL and DJJvH acknowledge NWO Vici grant 865.17.001 to DJJvH. We extend our heartfelt gratitude to Mr. Amir Jalali Nejad, Mr. Amir Sahbaie, Mr. Shams Damani Gol, and Dr. Ali Ahmadi for their invaluable support during field trips and sample collection. We much appreciated the constructive and helpful reviews of Michael Bröcker and an anonymous reviewer, as well as editorial handling by Gideon Rosenbaum.

Open Research

Original data of bedding, thrusts and dike plane of the Sedeh Formation generated from this study are openly available in Rojhani, Emad (2024), “Rojhani et al. 2024”, Mendeley Data, V3, doi: 10.17632/hzcpdwrnhs.3, Licence: CC BY 4.0.

References

Abbakhsh, T. R., Shafaroudi, A. M., and Karimpour, M. (2018). Geology, mineralization, geochemistry, and petrology of monzodioritc dikes in Hatamabad copper occurrence, northeast of Qaen. *Iranian Journal of Crystallography and Mineralogy* 26, 32-46

Agard, P., Omrani, J., Jolivet, L., Whitechurch, H., Vrielynck, B., Spakman, W., Monié, P., Meyer, B., & Wortel, R. (2011). Zagros orogeny: A subduction-dominated process. *Geological Magazine*, *148*, 692–725.

Agard, P., Yamato, P., Jolivet, L., & Burov, E. (2009). Exhumation of oceanic blueschists and eclogites in subduction zones: Timing and mechanisms. *Earth-Science Reviews*, *92*, 53–79.

Akrami, M. A., Chaichi, Z., & Haddadan, M. (2005). Geological map of Abiz, scale 1:100,000. *Geological Survey of Iran.*

Alavi-Naini, M. (1980). Shahrakht geological quadrangle map. *Geological Survey of Iran.*

Alavi-Naini, M., & Behruzi, A. (1983). Gonabad geological quadrangle map. In *Geological Survey of Iran:* No. K6.

Allen, M. B. (2021). Arabia-Eurasia Collision. *Encyclopedia of Geology (2nd ed.). Elsevier Inc*.

https://doi.org/10.1016/b978-0-12-409548-9.12522-9

Angiboust, S., Agard, P., De Hoog, J. C. M., Omrani, J., & Plunder, A. (2013). Insights on deep, accretionary subduction processes from the Sistan ophiolitic "mélange" (Eastern Iran). *Lithos*, 156–159, 139–158.

Arjmandzadeh, R., Karimpour, M. H., Mazaheri, S. A., Santos, J. F., Medina, J. M., & Homam, S. M. (2011). Two-sided asymmetric subduction; implications for tectonomagmatic and metallogenic evolution of the Lut Block, eastern Iran. *Journal of Economic Geology*, *3*, 1–14.

Arvin, M. and Robinson, P.T. (1994). The petrogenesis and tectonic setting of lavas from the Baft ophiolitic mélange, southwest of Kerman, Iran. *Canadian Journal of Earth Sciences, 31*, 824-834.

Babazadeh, S. A., & De Wever, P. (2004). Age crétacé des radiolarites de Soulabest dans la suite ophiolitique d'Iran oriental. *Bulletin de La Societe Geologique de France*, *175*, 121–129.

Baes, M., Govers, R., and Wortel, R. (2011). Subduction initiation along the inherited weakness zone at the edge of a slab: Insights from numerical models. *Geophysical Journal International*, *184*, 991-1008.

Bagheri, S,, & Damani Gol, S. (2020). The eastern iranian orocline. *Earth-Science Reviews*, *210*, 123.

Bagheri, S., & Stampfli, G. M. (2008). The Anarak, Jandaq and Posht-e-Badam metamorphic complexes in central Iran: New geological data, relationships and tectonic implications. *Tectonophysics*, *451*, 123–155.

Baroz, F., Macaudiere, J., Montigny, R., Noghreyan, M., Ohnstetter, M., and Rocci, G. (1984). Ophiolites and related formations in the central part of the Sabzevar range (Iran) and possible geotectonic reconstructions. *Neues Jahrbuch für Geologie und Paläontologie. Abhandlungen*, *168*, 358-388.

Berberian, F., & Berberian, M. (1981). Tectono-plutonic episodes in Iran. In H. K. Gupta & F. M. Delani (Eds.), *Zagros; Hindu Kush; Himalaya: Geodynamic Evolution; Geodynamics Series* 3, 5–32. American Geophysical Union.

Berberian, M. (1973). Structural history of Lut Zone*. Geological Survey of Iran. In Tehran, Internal report.*

Berberian, M., & King, G. C. P. (1981). Towards a paleogeography and tectonic evolution of Iran. *Canadian Journal of Earth Sciences*, *18*, 210–265.

Berthiaux, A., Christmann, P., Fauvelet, E., Hatrival, J., Vaslet, D., and Vahdati Daneshmand, A. (1991) Quadrangle Geological Map of Qayen. Scale: 1/250 000, *Geological Survey of Iran Tehran*.

Biabangard, H., Begheri, S., & Karimzaie, J. A. (2020). Petrology and geochemistry of gabbro part of Samsour Ophiolite, South East of Iran. *Iranian Journal of Crystallography and Mineralogy*, *28*, 95–110.

Bina, M. M., Bucur, I., Prevot, M., Meyerfeld, Y., Daly, L., Cantagrel, J. M., & Mergoil, J. (1986). Palaeomagnetism, petrology and geochronology of tertiary magmatic and sedimentary units from Iran. *Tectonophysics*, *121*, 303–329.

Bonnet, G., Agard, P., Angiboust, S., Monié, P., Jentzer, M., Omrani, J., Whitechurch, H., & Fournier, M. (2018). Tectonic slicing and mixing processes along the subduction interface: the Sistan example (Eastern Iran). *Lithos, 310-311*, 269-287 .

Boulin, J. (1990). Neocimmerian events in Central and Western Afghanistan. *Tectonophysics*, *175*, 285–315.

Bröcker, M., Fotoohi Rad, G., Burgess, R., Theunissen, S., Paderin, I., Rodionov, N., & Salimi, Z. (2013). New age constraints for the geodynamic evolution of the Sistan Suture Zone, eastern Iran. *Lithos*, *170–171*, 17–34.

Bröcker, M., Hövelkröger, Y., Rad, G. F., Berndt, J., Scherer, E. E., Kurzawa, T., & Moslempour, M. E. (2022). The magmatic and tectono-metamorphic history of the Sistan suture zone, Iran: New insights into a key region for the convergence between the Lut and Afghan blocks. *Journal of Asian Earth Sciences, 236*, 105313.

Camp, V. E., & Griffis, R. J. (1982). Character, genesis and tectonic setting of igneous rocks in the Sistan Suture Zone, eastern Iran. *Lithos*, *15*, 221–239.

Conrad, G., Montigny, R., Thuizat, R., & Westphal, M. (1981). Tertiary and quaternary geodynamics of southern Lut (Iran) as deduced from palaeomagnetic, isotopic and structural data. *Tectonophysics*, *75*.

Davoudzadeh, M., Soffel, H., & Schmidt, K. (1981). On the rotation of the Central-East-Iran microplate. *Neues Jahrbuch Für Geologie Und Paläontologie - Monatshefte*, *1981*, 180–192.

Delaloye, M., & Desmons, J. (1980). Ophiolites and mélange terranes in Iran: A geochronological study and its paleotectonic implications. *Tectonophysics*, *68*, 83–111.

Delavari, M. (2013). Different geodynamic settings for Sistan Suture Zone ophiolitic units: discussion of textural evidences and mineral chemistry of crustal sequence ultramafic-mafic associations. *Petrology*, *4*, 39–58.

Delavari, M., Amini, S., Schmitt, A. K., McKeegan, K. D., & Mark Harrison, T. (2014). U-Pb geochronology and geochemistry of Bibi-Maryam pluton, eastern Iran: Implication for the late stage of the tectonic evolution of the Sistan Ocean. *Lithos*, *200–201*, 197–211.

Desmons, J., & Beccaluva, L. (1983). Mid-ocean ridge and island-arc affinities in ophiolites from Iran: Palaeographic implications. Complementary reference. *Chemical Geology*, *39*, 39–63.

Déverchère, J., Yelles, K., Domzig, A., Mercier de Lépinay, B., Bouillin, J. P., Gaullier, V., Bracène, R., Calais, E., Savoye, B., and Kherroubi, A. (2005). Active thrust faulting offshore Boumerdes, Algeria, and its relations to the 2003 Mw 6.9 earthquake. *Geophysical Research Letters, 32,* https://doi.org/10.1029/2004GL021646

Eftekhar-Nezhad, J., & Ruttner, A. (1977). Ferdows geological quadrangle map No. J6. *Geological Survey of Iran.*

Eftekhar-Nezhad, J., & Stöcklin, J. (1992). Birjand geological quadrangle map. In *Geological Survey of Iran: No. K8*.

Esmaeily, D., Nédélec, A., Valizadeh, M. V., Moore, F., & Cotten, J. (2005). Petrology of the Jurassic Shah-Kuh granite (eastern Iran), with reference to tin mineralization. *Journal of Asian Earth Sciences*, *25*, 961–980.

Fauvelet, E., & Eftekhar-Nezhad, J. (1990). Explanatory text of the Qayen quadrangle map 1:250,000. In *Geological Survey of Iran*.

Fotoohi Rad, G. R., Droop, G. T. R., Amini, S., & Moazzen, M. (2005). Eclogites and blueschists of the Sistan Suture Zone, eastern Iran: A comparison of P-T histories from a subduction mélange. *Lithos*, *84*, 1–24.

Fotoohi Rad, G. R., Droop, G. T. R., & Burgess, R. (2009). Early Cretaceous exhumation of high-pressure metamorphic rocks of the Sistan Suture Zone, eastern Iran. *Geological Journal*, *44*, 104–116.

Gass, I. G. (1977). The evolution of the Pan African crystalline basement in NE Africa and Arabia. *Journal of the Geological Society*, *134*, 129–138.

Ghazi, A. M., Hassanipak, A. A., Mahoney,J. J., and Duncan, R. A. (2004) Geochemical characteristics, 40Ar–39Ar ages and original tectonic setting of the Band-e-Zeyarat/Dar Anar ophiolite, Makran accretionary prism, S.E. Iran. *Tectonophysics*, *393*, 175-196.

Gholami, N., Bagheri, S., & Heyhat, M. R. (2015). The Intruduction of the Ark nappe-thrust: a different glance at the tectonics of the northwest of the Birjand. *18th Symposium of Geological Society of Iran*. https://civilica.com/doc/391424

Girardeau, J., Marcoux, J., & Montenat, C. (1989). The Neo-Cimmerian Ophiolite Belt in Afghanistan and Tibet: Comparison and Evolution. *Tectonic Evolution of the Tethyan Region*, 477–504.

Govers, R., and Wortel, M. (2005). Lithosphere tearing at STEP faults: Response to edges of subduction zones. *Earth and Planetary Science Letters*, *236*, 505-523.

Griffin, W. (2008). GLITTER: data reduction software for laser ablation ICP-MS. *Laser Ablation ICP-MS in the Earth Sciences: Current practices and outstanding issues*, 308-311.

Guillou, Y., Maurizot, P., Vaslet, D., & Villéon, H. (1983). Gazik geological quadrangle map. In *Geological Survey* *of Iran: Vol. 1/250000* (Issue 250).

Hassanzadeh, J. & Wernicke, B. P. (2016). The Neo-Tethyan Sanandaj-Sirjan zone of Iran as an archetype for passive margin-arc transitions. *Tectonics 35*, 586-621.

Hollingsworth, J., Fattahi, M., Walker, R., Talebian, M., Bahroudi, A., Bolourchi, M.J., Jackson, J. and Copley, A., 2010. Oroclinal bending, distributed thrust and strike-slip faulting, and the accommodation of Arabia–Eurasia convergence in NE Iran since the Oligocene. *Geophysical Journal International*, *181*, 1214-1246.

Isozaki, Y., Maruyama, S., and Furuoka, F. (1990). Accreted oceanic materials in Japan. *Tectonophysics*, *181*, 179-205.

Jackson, J., & McKenzie, D. (1984). Active tectonics of the Alpine—Himalayan Belt between western Turkey and Pakistan. *Geophysical Journal International*, *77*, 185–264.

Jentzer, M., Agard, P., Bonnet, G., Monié, P., Fournier, M., Whitechurch, H., Omrani, J., Zarrinkoub, M. H., Khatib, M. M., Kohansal, R., Couto, D. Do, Godbillot, C., & Ninkabou, D. (2022). The North Sistan orogen (Eastern Iran): Tectono-metamorphic evolution and significance in the Tethyan realm. *Gondwana Research*, *109,* 460-492.

Jentzer, M., Whitechurch, H., Agard, P., Ulrich, M., Caron, B., Zarrinkoub, M. H., Kohansal, R., Miguet, L., Omrani, J., & Fournier, M. (2020). Late Cretaceous calc-alkaline and adakitic magmatism in the Sistan Suture Zone (Eastern Iran): Implications for subduction polarity and regional tectonics. *Journal of Asian Earth Sciences*, *204*, 104588.

Kapp, P., and DeCelles, P. G. (2019). Mesozoic–Cenozoic geological evolution of the Himalayan-Tibetan orogen and working tectonic hypotheses. *American Journal of Science*, *319*, 159-254.

Karimpour, M. H., Stern, C., Farmer, L., & Saadat, S. (2011). Review of age, Rb-Sr geochemistry and petrogenesis of Jurassic to Quaternary igneous rocks in Lut Block, Eastern Iran. *Geopersia*, *1*, 19–54.

Karimzadeh, H., Rahgoshay, M., & Monsef, I. (2020). Mineralogy, geochemistry and petrogenesis of mantle peridotites of nehbandan ophiolitic complex, east of Iran. *Journal of Economic Geology*, *12*, 157–176.

Keshtgar, S., Bagheri, S., & Boomeri, M. (2016). Tectonic history of the Mahi Rud (Cheshme-ostad) complex according to new structural data, East of Iran. *Journal of Tectonics*, *1*, 63–76.

Kluyver, M. H., Tirrul, R., Chance, P. N., Johns, G. W., & Mexiner, H. M. (1983). *Explanatory text of the Naybandan quadrangle map 1250,000* (No. J8). Geological Survey of Iran.

Kokaly, R. F., King, T. V. V.., & Hoefen, T. M. (2013). Surface Mineral Maps of Afghanistan Derived from HyMap Imaging Spectrometer Data, Version 2 *(Issue 186, p. 36). US Department of the Interior, US Geological Survey.*

Krumsiek, K. (1976). Zur Bewegung der Iranisch-Afghanischen Platte. *Geologische Rundschau*, *65*, 909–929.

Kurzawa, T., Bröcker, M., Fotoohi Rad, G., Berndt, J., & Lisker, F. (2017). Cretaceous high-pressure metamorphism and low-pressure overprint in the Sistan Suture Zone, eastern Iran: Additional temperature estimates for eclogites, geological significance of U-Pb zircon ages and Rb-Sr constraints on the timing of exhumation. *Journal of Asian Earth Sciences*, *147*, 332–344.

Latifi, Z., Foroughi, F., Motamedalshariati, M., & Raeisossadat, S. N. (2018). Calcareous nannofossils biostratigraphy of Lower Cretaceous deposits of east of Iran, NW of Qayen (Nimbolook stratigraphic section). *Journal of Geoscience*, *27*, 41–50.

Li, S., Advokaat, E. L., van Hinsbergen, D. J. J., Koymans, M., Deng, C., & Zhu, R. (2017). Paleomagnetic constraints on the Mesozoic-Cenozoic paleolatitudinal and rotational history of Indochina and South China: Review and updated kinematic reconstruction. *Earth-Science Reviews*, *171*, 58–77.

Lyberis, N. and Manby, G., 1999. Oblique to orthogonal convergence across the Turan block in the post-Miocene. *AAPG bulletin,* 83, pp.1135-1160.

Mattei, M., Cifelli, F., Muttoni, G. and Rashid, H., 2015. Post-Cimmerian (Jurassic–Cenozoic) paleogeography and vertical axis tectonic rotations of Central Iran and the Alborz Mountains. *Journal of Asian Earth Sciences*, *102*, 92-101.

Mattei, M., Cifelli, F., Muttoni, G., Zanchi, A., Berra, F., Mossavvari, F. and Eshraghi, S.A. (2012). Neogene block rotation in central Iran: Evidence from paleomagnetic data. *Geological Society of America Bulletin*, 124,943-956.

Maurizot, P. (1980). Explanatory text of the Gazik quadrangle map 1:250,000. *Geological Survey of Iran.*

Maurizot, P., Fauvelet, E., & Eftekhar-Nezhad, J. (1990). Explanatory text of the Shahrakht quadrangle map 1:250,000. *Geological Survey of Iran.*

McCall, G. J. (2002). A summary of the geology of the Iranian Makran. *Geological Society, London, Special Publications*, *195*, 147-204.

McQuarrie, N., & Van Hinsbergen, D. J. J. (2013). Retrodeforming the Arabia-Eurasia collision zone: Age of collision versus magnitude of continental subduction. *Geology*, *41*, 315–318.

Montenat, C. (2009). The Mesozoic of Afghanistan. *GeoArabia*, *14*, 147–210.

Moradi Noghondar, M., Karimpour, M., Farmer, G., & Stern, C. (2011). SrNd isotopic characteristic, U-Pb zircon geochronology, and petrogenesis of Najmabad Granodiorite batholith, Eastern Iran. *Journal of Economic Geology*, *3*, 127–145.

Moslempour, M. E., Khalatbari-jafari, M., & Dabiri, R. (2012). Constraints on the Petrogenesis of Nosrat-Abad Ophiolite. *Iranian Journal of Earth Sciences, 4*, 125-133.

Nikbakht, S., Biabanghard, H., & Bagheri, S. (2021). Petrology and geochemistry of Siahjangal ophiolite, northeastern Taftan volcano. *Iranian Journal of Geology, 56*, 87.

Ozsvárt, P., Bahramnejad, E., Bagheri, S., & Sharifi, M. (2020). New Albian (Cretaceous) radiolarian age constraints for the Dumak ophiolitic mélange from the Shuru area, Eastern Iran. *Cretaceous Research*, *111*, 104451.

Pang, K. N., Chung, S. L., Zarrinkoub, M. H., Khatib, M. M., Mohammadi, S. S., Chiu, H. Y., Chu, C. H., Lee, H. Y., & Lo, C. H. (2013). Eocene-Oligocene post-collisional magmatism in the Lut-Sistan region, eastern Iran: Magma genesis and tectonic implications. *Lithos*, *180–181*, 234–251.

Pang, K. N., Chung, S. L., Zarrinkoub, M. H., Mohammadi, S. S., Yang, H. M., Chu, C. H., Lee, H. Y., & Lo, C. H. (2012). Age, geochemical characteristics and petrogenesis of Late Cenozoic intraplate alkali basalts in the Lut-Sistan region, eastern Iran. *Chemical Geology*, *306–307*, 40–53.

Pastor-Galán, D., Mulchrone, K. F., Koymans, M. R., van Hinsbergen, D. J. J., and Langereis, C. G. (2017). Bootstrapped total least squares orocline test: A robust method to quantify vertical-axis rotation patterns in orogens, with examples from the Cantabrian and Aegean oroclines. *Lithosphere*, *9*, 499-511.

Pirnia, T., Saccani, E., Torabi, G., Chiari, M., Goričan, Š., and Barbero, E. (2020). Cretaceous tectonic evolution of the Neo-Tethys in Central Iran: Evidence from petrology and age of the Nain-Ashin ophiolitic basalts. *Geoscience Frontiers*, *11*, 57-81.

Raisossadat, S. N., Mosavinia, A., khazaei, A., & Asadi, S. (2020). Biostratigraphy of Cretaceous deposits based on ammonites in Southwest of Qayen area (Qumenjan section). *Journal of Stratigraphy and Sedimentology Researches, 37*, 127-146.

Ratschbacher, Lothar, Merle, O., Davy, P., & Cobbold, P. (1991). Lateral extrusion in the eastern Alps, Part 1: Boundary conditions and experiments scaled for gravity. *Tectonics*, *10*, 245–256.

https://doi.org/10.1029/90TC02622

Robinson, A. C. (2015). Mesozoic tectonics of the Gondwanan terranes of the Pamir plateau. *Journal of Asian Earth Sciences*, *102*, 170-179.

Rossetti, F., Nasrabady, M., Vignaroli, G., Theye, T., Gerdes, A., Razavi, M. H., & Vaziri, H. M. (2010). Early Cretaceous migmatitic mafic granulites from the Sabzevar range (NE Iran): Implications for the closure of the Mesozoic peri-Tethyan oceans in central Iran. *Terra Nova*, *22*, 26–34.

Rossetti, F., Nasrabady, M., Theye, T., Gerdes, A., Monie, P., Lucci, F., and Vignaroli, G. (2014). Adakite differentiation and emplacement in a subduction channel: The late Paleocene Sabzevar magmatism (NE Iran): *Geological Society of America Bulletin*, *126*, 317-343.

Rowshanravan, J., Shojai kaveh, N., & Bahremand, M. (2006). 1: 100000 Geological map of Mousaviyeh. In *Geological Survey of Iran*.

Saccani, E., Delavari, M., Beccaluva, L., & Amini, S. (2010). Petrological and geochemical constraints on the origin of the Nehbandan ophiolitic complex (eastern Iran): Implication for the evolution of the Sistan Ocean. *Lithos*, *117*, 209–228.

Sargazi, M., Bagheri, S., & Ma, X. (2022). Oligocene calc-alkaline lamprophyres and K-rich association in the eastern Iranian ranges: Products of low-degree melting of subduction-modified lithospheric mantle in post-orogenic setting. *Lithos*, *430–431*, 106864.

Schreiber, A., Weippert, D., Wittekindt, H. P., & Wolfart, R. (1972). Geology and Petroleum Potentials of Central and South Afghanistan. *American Association of Petroleum Geologists Bulletin*, *56*, 1494–1519.

Şengör, A. M. C. (1979). Mid-Mesozoic closure of Permo-Triassic Tethys and its implications. *Nature*, *279*, 590–593.

Şengör, A. M. C. (1984). The cimmeride orogenic system and the tectonics of Eurasia. *Special Paper of the Geological Society of America*, *195*, 1–74.

Şengör, A.M.C., Altıner, D., Zabcı, C., Sunal, G., Lom, N., Aylan, E., Öner, T. (2023). On the nature of the Cimmerian Continent. *Earth-Science Reviews, 247*, 104520.

Shojaat, B., Hassanipak, A., Mobasher, K., and Ghazi, A. (2003) Petrology, geochemistry and tectonics of the Sabzevar ophiolite, North Central Iran. *Journal of Asian Earth Sciences*, *21*, 1053-1067.

Siehl, A. (2017). Structural setting and evolution of the Afghan orogenic segment - A review. *Geological Society,* *London, Special Publication, 427*, 57–88).

Soffel, H. C., Davoudzadeh, M., & Rolf, C. (1992). A new polar wander path of the Central East Iran Microplate (CEIM) and its tectonic interpretation. *Geosci Sci QJ Geol Surv Iran*, *2*, 2–24.

Soffel, H. C., Davoudzadeh, M., Rolf, C., & Schmidt, S. (1996). New palaeomagnetic data from Central Iran and a Triassic palaeoreconstruction. *Geologische Rundschau*, *85*, 293–302.

Soffel, H.C. and Förster, H.G., 1980. Apparent polar wander path of Central Iran and its geotectonic interpretation. *Journal of geomagnetism and geoelectricity*, *32*, SIII117-SIII135.

Soffel, H. C., & Förster, H. G. (1984). Polar Wander Path of the Central-East-Iran Microplate Including New Results. *Neues Jahrbuch Für Geologie Und Paläontologie - Abhandlungen*, *168*, 165–172.

Spakman, W., and Wortel, R. (2004). A Tomographic View on Western Mediterranean Geodynamics, *in* Cavazza, W., Roure, F., Spakman, W., Stampfli, G. M., and Ziegler, P. A., eds., The TRANSMED Atlas. The Mediterranean Region from Crust to Mantle: Geological and Geophysical Framework of the Mediterranean and the Surrounding Areas: Berlin, Heidelberg, Springer Berlin Heidelberg, p. 31-52.

Stampfli, G. M., Marcoux, J., & Baud, A. (1991). Tethyan margins in space and time. *Palaeogeography, Palaeoclimatology, Palaeoecology*, *87*, 373–409.

Stöcklin, J. (1968). Structural History and Tectonics of Iran. *American Association of Petroleum Geologists Bulletin*, *52*, 1229–1258.

Stöcklin, J. (1974). Possible Ancient Continental Margins in Iran. *The Geology of Continental Margins*, 873–887.

Stöcklin, Johan, & Mabavi, M. H. (1973). *Tectonic map of Iran*. Geological Survey of Iran.

Stöcklin, Jovan. (1981). A brief report on geodynamics in Iran. *Zagros Hindu Kush Himalaya Geodynamic Evolution*, *3*, 70–74.

Stöcklin, Jovan. (1989). Tethys Evolution in the Afghanistan-Pamir Region. *Tectonic Evolution of the Tethyan Region*, *25*, 241–264.

Tapponnier, P., Mattauer, M., Proust, F. & Cassaigneau, C. (1981). Mesozoic ophiolites, sutures, and large-scale tectonic movements in Afghanistan. *Earth and Planetary Science Letters*, 52, 355-71.

Tapponnier, P., Peltzer, G., Le Dain, A. Y., Armijo, R., & Cobbold, P. (1982). Propagating extrusion tectonics in Asia: new insights from simple experiments with plasticine. *Geology*, *10*, 611–616.

Tarkian, M., Lotfi, M., & Baumann, A. (1983). *Tectonic, magmatism and the Formation of mineral deposits in the* *central Lut, east Iran*.

Tirrul, R., Bell, I. R., Griffis, R. J., & Camp, V. E. (1983). The Sistan Suture Zone of eastern Iran. *Geological Society of America Bulletin*, *94*, 134–150.

Tirrul, R., Griffis, R. J., & Camp, V. E. (1980). Geology of the Zabol Quadrangle, 1.250, 000. In *Geological Survey of Iran* (Vol. 180).

van Hinsbergen, D. J. J., Vissers, R. L. M., and Spakman, W. (2014). Origin and consequences of western Mediterranean subduction, rollback, and slab segmentation. *Tectonics*, *33*, 393-419.

Vermeesch, P. (2012). On the visualisation of detrital age distributions. *Chemical Geology*, 312, 190-194.

Walker, R., & Jackson, J. (2004). Active tectonics and late Cenozoic strain distribution in central and eastern Iran. *Tectonics*, *23*, 1–24.

Wu, F.-Y., Yang, Y.-H., Marks, M. A., Liu, Z.-C., Zhou, Q., Ge, W.-C., Yang, J.-S., Zhao, Z.-F., Mitchell, R. H., and Markl, G. (2010). In situ U–Pb, Sr, Nd and Hf isotopic analysis of eudialyte by LA-(MC)-ICP-MS. *Chemical Geology*, *273*, 8-34.

Yin, A. and T. M. Harrison (2000). Geologic evolution of the Himalayan-Tibetan orogen. *Annual Review of Earth and Planetary Sciences, 28*, 211-280.

Zarrinkoub, M. H., Pang, K. N., Chung, S. L., Khatib, M. M., Mohammadi, S. S., Chiu, H. Y., & Lee, H. Y. (2012). Zircon U-Pb age and geochemical constraints on the origin of the Birjand ophiolite, Sistan Suture Zone, eastern Iran. *Lithos*, *154*, 392–405.